A&A 389, 641–664 (2002)
DOI: 10.1051/0004-6361:20020431

Astronomy & Astrophysics

Colors of Minor Bodies in the Outer Solar System⋆,⋆⋆

A statistical analysis

O. R. Hainaut[1] and A. C. Delsanti[1,2]

[1] European Southern Observatory, Casilla 19001, Santiago, Chile
[2] Observatoire de Paris-Meudon, 5 place Jules Janssen, 92195 Meudon Cedex, France

Received 12 October 2001 / Accepted 14 February 2002

Abstract. We present a compilation of all available colors for 104 Minor Bodies in the Outer Solar System (MBOSSes); for each object, the original references are listed. The measurements were combined in a way that does not introduce rotational color artifacts. We then derive the slope, or reddening gradient, of the low resolution reflectance spectra obtained from the broad-band color for each object. A set of color-color diagrams, histograms and cumulative probability functions are presented as a reference for further studies, and are discussed. In the color-color diagrams, most of the objects are located very close to the "reddening line" (corresponding to linear reflectivity spectra). A small but systematic deviation is observed toward the I band indicating a flattening of the reflectivity at longer wavelengths, as expected from laboratory spectra. A deviation from linear spectra is noticed toward the B for the bluer objects; this is not matched by laboratory spectra of fresh ices, possibly suggesting that these objects could be covered with extremely evolved/irradiated ices. Five objects (1995 SM_{55}, 1996 TL_{66}, 1999 OY_3, 1996 TO_{66} and (2060) Chiron) have almost perfectly solar colors; as two of these are known or suspected to harbour cometary activity, the others should be searched for activity or fresh ice signatures. In the color-color diagrams, 1994 ES_2, 1994 EV_3, 1995 DA_2 and 1998 HK_{151} are located very far from the main group of objects; it is suspected that this corresponds to inaccurate measurements and not intrinsically strange objects. The color distributions were analyzed as functions of the orbital parameters of the objects and of their absolute magnitude. No significant correlation is observed, with the following exceptions: Cubewanos with low orbital excitation (low i, e and/or $\mathcal{E} = \sqrt{e^2 + \sin^2 i}$), and therefore experiencing on average fewer and less violent collisions have significantly redder colors; Cubewanos with faint absolute magnitude $M(1,1)$ tend to be redder than the others, while Plutinos present the opposite trend. The color distribution of the various MBOSS classes are analyzed and compared using generic statistic tools. The comets were found to be significantly bluer than the other MBOSSes. Finally, we compare the various 1D and 2D color distributions to simple models, in order to throw some light on the question of the bimodality of MBOSS color distributions. It is found that with the current data set, all color distributions are compatible with simple, continuous distribution models, while some color distributions are not compatible with simple bimodal distribution models. Table 1 is also available in electronic form at the CDS via anonymous ftp to `cdsarc.u-strasbg.fr (130.79.128.5)` or via `http://cdsweb.u-strasbg.fr/cgi-bin/qcat?J/A+A/389/641`, and the tables and complete set of figures corresponding the up-to-date database are available on the web at `http://www.sc.eso.org/~ohainaut/MBOSS`.

Key words. comets: general – Kuiper Belt – solar system: general – methods: statistical

1. Introduction

As soon as colors were available for a few Transneptunian Objects (TNOs), it was very tempting to see families and groups in the various color and color-color diagrams. Immediately after the discovery of 1992 QB_1, D. Jewitt presented a thorough analysis of *one* data point (Jewitt 1992), with the un-attackable argument that for years, people had done similarly detailed analysis on *zero* data points. The first detailed analysis was published by the Hawaii group (Luu & Jewitt 1996a). In the following years, with the continuous increase of the data set available, more analyses were published, but they are usually over-exploiting the data, without much consideration for the statistical significance of their (otherwise interesting) claims.

The physical properties of TNOs are difficult to assess; indeed, their faint magnitudes prevent them from

Send offprint requests to: O. R. Hainaut,
e-mail: `ohainaut@eso.org`

⋆ Table 1 is also available in electronic form at the CDS via anonymous ftp to `cdsarc.u-strasbg.fr (130.79.128.5)` or via `http://cdsweb.u-strasbg.fr/cgi-bin/qcat?J/A+A/389/641`

⋆⋆ Tables 3, 5, 6 and the list of papers are only available in electronic form at `http://www.edpsciences.org`

being studied in detail using the arsenal of observation techniques that could be used were they brighter. Only a handful of them were observed spectroscopically; the spectra reveal continuous, featureless gradients in the visible (e.g. Boehnhardt et al. 2001; Davies 2000), and a fairly flat spectrum in the near-IR (e.g. Davies 2000; Brown et al. 1998; McBride et al. 1999; Brown et al. 1999), in some cases displaying water absorption bands (e.g. Brown et al. 1999). The bulk of physical studies comes from Visible and/or IR colors.

1.1. Dynamical families and their inter-connections

This section gives a broad overview of the connections between the different classes of MBOSSes. We keep this introduction to the minimum: it is not meant as a review of this quickly evolving field. It is now broadly accepted that the TNOs constitute the largest members of the Edgeworth-Kuiper belt, which is in turn a remnant of the proto-planetary nebula extending beyond the region where planets formed. In that region, the small quantity of material available and the fairly quiet dynamical environment prevented the formation of planet-sized bodies. The "Main Belt" TNOs, also called Cubewanos (for 1992 QB_1, the first discovered, Jewitt & Luu 1992) or "Classical TNOs", are found on orbits of low/moderate eccentricity and inclinations with semi-major axis >40 AU. Their orbital parameters are not primordial, as they are still in the influence area of the outer planets. Beyond 45 AU, i.e. where the gravitational field of the planets has no effects anymore, it is hypothesized that there could lie a very thin belt of smaller objects with a dynamically very cold –and primordial– orbit distribution, forming the "Cold Disk" (Hahn 2000). This class has not been identified observationally yet. Other dynamicists (e.g. Morbidelli 2001) can explain the observed distribution of MBOSSes without the need for such a Cold Disk.

During the latest stages of the planetary accretion, the proto-Uranus and Neptune scattered a significant number of proto-planetesimals (Malhotra 1995). According to some dynamicists (Malhotra 1996; Hahn & Malhotra 1999), this caused their orbit semi-major axis to increase, the so-called planet migration. In that process, the orbital resonances associated with Neptune swept the inner part of the Edgeworth-Kuiper Belt, trapping the objects whose orbit passed through the resonance. The orbit of these objects were excited in e and i, eccentricity and inclination, resp. (Malhotra 1995; Malhotra 1996; Hahn & Malhotra 1999). Objects from this class are known as "Resonant TNOs", or Plutinos, after the most famous of their members, Pluto. For other dynamicists (Morbidelli 2001), planet migration is not needed to explain the population of the orbital resonances.

Some of the TNOs from the inner Kuiper Belt are on orbits that are unstable over the age of the Solar System because of interactions with Uranus and Neptune. Because of these instabilities, there is a continuous flow of such objects toward the Jupiter-Saturn region, where they can stay for a few million years (Kowal et al. 1979; Asher & Steel 1993). Thanks to their proximity to the Sun, they can develop a significant cometary activity, as it was the case for the first object discovered in this class: Chiron (Kowal 1977; Kowal et al. 1979).

In his history of outer Solar System astronomy, Davies (2001) explains that "Kowal looked for a group of mythological characters unrepresented amongst the asteroids. He found the Centaurs, strange creatures, half human and half horses". His choice was a very good one, as it also fits their dual appearance, half comet, half asteroid.

Through the interactions with Uranus and Neptune, some TNOs are also ejected on very eccentric, very elongated orbits with large semi-major axis a; these are called "Scattered TNOs". The dynamical distinction between Centaurs and Scattered TNOs is not very clear; the classification is based on their orbit semi-major axis, the limit being loosely defined. In this paper, we define objects from this class with $a < 35$ as Centaurs, those with larger a, as Scattered TNOs.

Finally, as their orbits are not stable, some of the Centaurs can fall further toward the inner solar system, where they will appear as Short Period (SP) Comets (Kowal et al. 1979); for instance, simulation by Asher & Steel (1993) showed that ∼20% of the test particles originally on Pholus-like orbit would end up on comet-like orbits. Nevertheless, the main source of short period comets is believed to be directly the inner Kuiper Belt; a very efficient way to transfer objects from that region to comet-like orbit is through collisions. It is estimated that ∼90% of the SP comets originating from the Kuiper Belt correspond to collisional fragments that were directly ejected from the Belt (Farinella & Davis 1996).

1.2. Physical properties

From a physical point of view, Cubewanos, Plutinos, Scattered TNOs, Centaurs and SP Comets (i.e. Minor Bodies in the Outer Solar System, MBOSS) are closely related, and are all believed to have the Edgeworth-Kuiper Belt as a common origin. It is therefore quite natural to consider that they have the same intrinsic physical nature. Nevertheless, their current location and past history may have affected them in different ways.

The MBOSSes cover a broad range of colors, from neutral (solar colors), possibly slightly bluish to very red (see, for instance, Jewitt & Luu 1998; Boehnhardt et al. 2001; Delsanti et al. 2001) for the TNOs, Meech et al. (2002) for the SP comets. Three main phenomena are suspected to contribute to this color diversity:

– Aging: considering that their surface is likely to be covered with organic-rich water ice, irradiation of the surface layers by high-energy particles (cosmic rays, hard UV...) will cause the organic molecules to lose Hydrogen atoms, and a progressive polymerization. This results in a slow, progressive reddening of

the object, with a time-scale of $10^{\sim 7}$ yrs, the blue albedo decreasing down to a few percent (Strazzula & Johnhson 1991; Strazzula 1998). With further irradiation, the icy surface is expected to become dark grey (uniform albedo of a few percent), with a time-scale ten times longer (Thompson et al. 1987);
- Impact on the surface will also alter the color of the object by exposing underlying, non-irradiated (and neutral-bluish) material. The frequency of these impacts will differ considerably depending on the region of the MBOSS being considered. The collisions in the Edgeworth-Kuiper Belt have been studied in detail (Stern 1996; Davis & Farinella 1997);
- Cometary activity is also expected to alter the object color, as it removes the upper layer of the active regions and deposits fresh dust on the surface, which is likely to make it neutral to blue. While cometary activity obviously has an effect on comets, it must also be considered for Centaurs, as exemplified by (2060) Chiron. Recent observations also suggest that the cometary activity could play a role for TNOs (Hainaut et al. 2000; Sekiguchi et al. 2002).

It is also interesting to note that the laboratory experiments simulating the object surface for different irradiation levels (i.e. different ages) all present fairly linear spectra over the visible wavelengths, but with changing slope (Thompson et al. 1987). The three phenomena described above will produce a variegated object, with regions of different ages, each of them presenting a different spectrum, hence a different color. However, the average spectrum over the surface being the average of linear spectra with different slopes, this total spectrum is expected also to be linear over the visible wavelength range.

While the reddening by irradiation will affect all MBOSSes in a similar way (to some extent, see Thompson et al. 1987), the time scale for collision re-surfacing will be very different for the different classes. Similarly, the importance of the cometary activity will be a function of the heliocentric distance of the object. The thickness of the irradiation crust and/or of a dust mantle will also determine whether an object is active or not; the impact rate will therefore be linked to the cometary activity. The different MBOSS populations will therefore be affected – at least – by these three phenomena, but the equilibrium between them will be different, resulting in different color distributions. The balance between collisions and reddening has been studied numerically in the case of TNOs (Luu & Jewitt 1996a). The model used was fairly simple – in particular, it did not take into account the darkening of the surface that follows the reddening, but could reproduce the color diversity observed. One can hope that it will become possible to use the observed color distributions to further constrain the relative importance of the evolution phenomena for the different MBOSSes.

Recent papers have been published discussing fairly large samples of TNOs; while some authors see these objects evenly spread over the whole color range (Barucci et al. 2000; Boehnhardt et al. 2001; Delsanti et al. 2001; Davies 2000), others have reported that the TNO population is distributed into two well separated color classes: one of solar color, the other very red (Tegler & Romanishin 1998). It is intriguing that different groups obtain such different results. We will investigate whether this can be a random, selection effect, or if other conclusions have to be reached.

1.3. Structure of this paper

The purposes of this paper are the following:

- In Sect. 2, we will first give a description of the individual objects that is as complete as possible, based on all the published photometric information. For each object, we will compute the "reddening", or spectral gradient, which describes the global slope of the reflectance spectrum;
- In Sect. 3, we will look for correlations between the objects' surface characteristics and size, orbital parameters, etc.;
- Section 4 is devoted to the description of individual classes of objects;
- In Sect. 5, we will compare the data of the different MBOSS classes, in order to cast some light on their similarities and differences.
- Finally, in Sect. 6, we will compare the colors of the various MBOSS classes with simple models, in order to investigate the reality of their possible bimodal or continuous distribution.

In these sections, we will each time highlight the results of the individual tests and give the conclusions that can be drawn from them taken individually.

We will then discuss the results from a more general point of view and summarize them in Sect. 7. Most of the tables and plots shown in this paper are directly generated from the measurement database (described later on). We intend to keep this database up-to-date (contributions from measurers are welcome), to make it available as a web page and, if needed, publish updates of this analysis every time the size of the studied population is multiplied by 2–3, i.e. when we can expect a major step in significance of the results described. Finally, in Appendix A, we give the complete list of reference for each objects. We also give there a fairly detailed description of the statistical tests used in the paper and the numerical results of these tests. It is recommended that the reader who is not familiar with these techniques read the Appendix first. The present paper represent a snapshot of the color database, which is continuously growing. Up-to-date versions of the tables and figures, as well as many additional figures, are available on our web site at `http://www.sc.eso.org/~ohainaut/MBOSS`.

Table 1. Average magnitudes and colors; online version at CDS, and an updated version is available on-line at http://www.sc.eso.org/~ohainaut/MBOSS.

Object	(1)/(2)	M11 $\pm\sigma$	Grt $\pm$ σ	$B-V \pm \sigma$	$V-R \pm \sigma$	$R-I \pm \sigma$	$I-J \pm \sigma$	$J-H \pm \sigma$	$H-K \pm \sigma$
2060 Chiron	Cent/27	6.398 ± 0.049	0.642 ± 1.629	0.679 ± 0.039	0.359 ± 0.027	0.356 ± 0.037	0.472 ± 0.132	0.290 ± 0.082	0.064 ± 0.099
5145 Pholus	Cent/36	7.158 ± 0.097	52.054 ± 2.105	1.299 ± 0.099	0.794 ± 0.032	0.814 ± 0.056	1.040 ± 0.051	0.375 ± 0.046	−0.037 ± 0.047
7066 Nessus	Cent/17	—	45.727 ± 2.567	1.090 ± 0.040	0.793 ± 0.041	0.695 ± 0.066	0.790 ± 0.122	0.309 ± 0.268	−0.089 ± 0.385
8405 Asbolus	Cent/34	8.966 ± 0.057	15.075 ± 2.981	0.750 ± 0.040	0.513 ± 0.068	0.523 ± 0.045	0.690 ± 0.056	0.315 ± 0.142	0.095 ± 0.253
10199 Chariklo	Cent/38	6.486 ± 0.033	13.677 ± 1.548	0.802 ± 0.049	0.479 ± 0.029	0.542 ± 0.030	0.730 ± 0.040	0.411 ± 0.044	0.093 ± 0.046
10370 Hylonome	Cent/7	—	10.667 ± 4.090	0.643 ± 0.082	0.464 ± 0.059	0.490 ± 0.122	0.390 ± 0.173	—	—
2P/Encke	SPC/4	—	3.770 ± 3.070	—	0.388 ± 0.062	0.408 ± 0.060	—	—	—
6P/d'Arrest	SPC/2	—	15.138 ± 2.886	0.770 ± 0.040	0.565 ± 0.067	0.450 ± 0.040	—	—	—
10P/Tempel 2	SPC/2	—	—	—	0.575 ± 0.048	—	—	—	—
22P/Kopff	SPC/1	—	—	—	0.533 ± 0.022	—	—	—	—
28P/Neujmin 1	SPC/6	—	11.687 ± 3.947	—	0.508 ± 0.079	0.440 ± 0.079	—	—	—
46P/Wirtanen	SPC/1	—	—	—	0.355 ± 0.073	—	—	—	—
53P/VanBiesbroek	SPC/1	—	—	—	0.328 ± 0.081	—	—	—	—
86P/Wild3	SPC/1	—	—	—	0.116 ± 0.144	—	—	—	—
87P/Bus	SPC/1	—	—	—	0.543 ± 0.020	—	—	—	—
93K2P/Helin-Law.	SPC/1	—	—	—	0.267 ± 0.075	—	—	—	—
96P/Machholz 1	SPC/1	—	—	—	0.429 ± 0.027	—	—	—	—
107P/Wilson-Harr.	SPC/2	—	—	—	0.406 ± 0.017	—	—	—	—
143P/Kowal-Mrkos	SPC/2	—	20.983 ± 1.167	0.820 ± 0.028	0.580 ± 0.020	0.560 ± 0.022	—	—	—
1992 QB_1	QB1/8	6.864 ± 0.121	37.328 ± 6.651	0.836 ± 0.145	0.713 ± 0.098	0.672 ± 0.197	—	—	—
1993 FW	QB1/8	6.533 ± 0.151	12.172 ± 5.517	0.932 ± 0.089	0.517 ± 0.101	0.431 ± 0.127	—	—	—
1993 RO	Plut/6	8.488 ± 0.113	19.363 ± 7.579	0.933 ± 0.162	0.576 ± 0.128	0.515 ± 0.192	—	—	—
1993 SB	Plut/4	8.024 ± 0.143	12.253 ± 4.554	0.802 ± 0.071	0.475 ± 0.077	0.514 ± 0.114	—	—	—
1993 SC	Plut/14	6.711 ± 0.054	36.763 ± 3.488	1.012 ± 0.105	0.673 ± 0.065	0.738 ± 0.077	—	0.400 ± 0.203	−0.040 ± 0.197
1994 ES_2	QB1/2	7.525 ± 0.115	80.403 ± 7.434	0.710 ± 0.150	0.940 ± 0.150	0.970 ± 0.150	—	—	—
1994 EV_3	QB1/4	7.108 ± 0.089	27.511 ± 7.555	1.500 ± 0.150	0.516 ± 0.124	0.840 ± 0.199	—	—	—
1994 GV_9	QB1/1	6.815 ± 0.091	—	—	0.740 ± 0.099	—	—	—	—
1994 JQ_1	QB1/5	6.603 ± 0.127	—	—	0.945 ± 0.097	—	—	—	—
1994 JR_1	Plut/7	6.844 ± 0.071	24.825 ± 5.805	1.010 ± 0.180	0.656 ± 0.115	0.520 ± 0.120	—	—	—
1994 JS	QB1/2	7.255 ± 0.062	—	—	0.850 ± 0.070	—	—	—	—
1994 JV	QB1/2	7.195 ± 0.058	37.024 ± 5.331	—	0.771 ± 0.091	0.563 ± 0.133	—	—	—
1994 TA	Cent/2	11.413 ± 0.126	35.801 ± 6.104	1.261 ± 0.139	0.672 ± 0.080	0.740 ± 0.210	—	—	—
1994 TB	Plut/10	7.505 ± 0.080	39.035 ± 4.615	1.080 ± 0.132	0.706 ± 0.083	0.727 ± 0.108	—	—	—
1994 VK_8	QB1/2	7.025 ± 0.144	32.582 ± 6.345	1.010 ± 0.060	0.659 ± 0.061	—	—	—	—
1995 DA_2	QB1/7	7.964 ± 0.118	17.189 ± 7.292	1.310 ± 0.270	0.547 ± 0.131	0.515 ± 0.172	—	—	—
1995 DB_2	QB1/2	8.112 ± 0.085	—	—	—	—	—	—	—
1995 DC_2	QB1/6	6.848 ± 0.148	36.530 ± 7.927	—	0.770 ± 0.160	0.580 ± 0.160	—	—	—
1995 FB_{21}	QB1/4	7.017 ± 0.099	—	—	—	—	—	—	—
1995 HM_5	Plut/7	7.881 ± 0.111	6.761 ± 4.993	0.649 ± 0.102	0.463 ± 0.096	0.370 ± 0.108	—	1.200 ± 0.470	—
1995 QY_9	Plut/6	7.487 ± 0.126	10.588 ± 4.022	0.696 ± 0.121	0.520 ± 0.093	0.400 ± 0.060	—	—	—
1995 QZ_9	Plut/2	7.886 ± 0.400	15.709 ± 5.234	0.880 ± 0.040	0.515 ± 0.050	—	—	—	—
1995 SM_{55}	QB1/3	4.333 ± 0.053	1.269 ± 2.875	0.645 ± 0.034	0.394 ± 0.052	0.310 ± 0.066	—	—	—
1995 TL_8	Scat/1	4.585 ± 0.056	33.942 ± 3.051	1.045 ± 0.072	0.695 ± 0.051	0.641 ± 0.076	—	—	—
1995 WY_2	QB1/3	6.861 ± 0.110	21.766 ± 9.753	1.004 ± 0.206	0.648 ± 0.190	0.458 ± 0.208	—	—	—
1996 RQ_{20}	QB1/5	6.890 ± 0.104	21.258 ± 5.329	0.935 ± 0.141	0.553 ± 0.099	0.609 ± 0.120	—	—	—
1996 RR_{20}	Plut/2	6.586 ± 0.133	40.209 ± 5.038	1.150 ± 0.094	0.707 ± 0.070	0.760 ± 0.160	—	—	—
1996 SZ_4	Plut/2	8.181 ± 0.159	19.062 ± 4.832	0.783 ± 0.124	0.531 ± 0.062	0.620 ± 0.170	—	—	—
1996 TC_{68}	QB1/1	6.734 ± 0.073	—	—	0.600 ± 0.078	—	—	—	—
1996 TK_{66}	QB1/2	6.281 ± 0.074	27.932 ± 3.716	1.002 ± 0.060	0.640 ± 0.050	0.590 ± 0.120	—	—	—
1996 TL_{66}	Scat/10	5.227 ± 0.133	3.355 ± 3.011	0.694 ± 0.056	0.334 ± 0.052	0.428 ± 0.079	—	0.350 ± 0.117	−0.040 ± 0.112
1996 TO_{66}	QB1/16	4.544 ± 0.049	5.371 ± 2.467	0.666 ± 0.060	0.377 ± 0.047	0.375 ± 0.060	—	−0.210 ± 0.170	0.810 ± 0.158
1996 TP_{66}	QB1/9	6.958 ± 0.063	32.326 ± 3.690	0.984 ± 0.109	0.654 ± 0.073	0.683 ± 0.075	—	0.170 ± 0.078	0.020 ± 0.092
1996 TQ_{66}	Plut/6	7.137 ± 0.078	35.809 ± 4.398	1.186 ± 0.118	0.655 ± 0.081	0.750 ± 0.100	—	—	—
1996 TS_{66}	QB1/9	5.986 ± 0.112	28.922 ± 5.214	1.010 ± 0.082	0.635 ± 0.110	0.645 ± 0.097	—	0.650 ± 0.071	—
1997 CQ_{29}	QB1/5	6.763 ± 0.183	34.308 ± 5.942	0.990 ± 0.127	0.728 ± 0.120	0.605 ± 0.120	—	—	—
1997 CR_{29}	QB1/2	7.076 ± 0.135	20.636 ± 8.257	0.750 ± 0.152	0.538 ± 0.157	0.620 ± 0.182	—	—	—
1997 CS_{29}	QB1/10	5.065 ± 0.085	28.988 ± 2.815	1.049 ± 0.082	0.667 ± 0.053	0.592 ± 0.061	—	0.300 ± 0.156	−0.100 ± 0.233
1997 CT_{29}	QB1/2	6.498 ± 0.230	—	—	0.744 ± 0.090	—	—	—	—
1997 CU_{29}	QB1/4	6.206 ± 0.108	28.730 ± 3.680	1.157 ± 0.145	0.634 ± 0.058	0.638 ± 0.098	—	—	—
1997 GA_{45}	QB1/1	7.744 ± 0.500	—	—	—	—	—	—	—
1997 QH_4	QB1/3	6.983 ± 0.133	28.694 ± 6.173	1.039 ± 0.131	0.628 ± 0.103	0.649 ± 0.159	—	—	—
1997 QJ_4	Plut/3	7.424 ± 0.124	9.307 ± 6.115	0.700 ± 0.120	0.511 ± 0.119	0.362 ± 0.130	—	—	—
1997 RL_{13}	QB1/1	9.361 ± 0.300	—	—	—	—	—	—	—
1997 RT_5	QB1/1	6.736 ± 0.030	—	—	—	—	—	—	—
1997 RX_9	QB1/1	7.800 ± 0.100	—	—	—	—	—	—	—
1997 SZ_{10}	QB1/1	8.145 ± 0.060	31.431 ± 3.246	1.140 ± 0.080	0.650 ± 0.030	—	—	—	—
1998 BU_{48}	Cent/1	7.033 ± 0.057	26.985 ± 3.102	1.105 ± 0.074	0.648 ± 0.052	0.570 ± 0.078	—	—	—
1998 FS_{144}	QB1/1	—	20.767 ± 6.964	0.910 ± 0.076	0.560 ± 0.067	—	—	—	—
1998 HK_{151}	Plut/3	6.879 ± 0.039	8.017 ± 3.404	0.510 ± 0.090	0.469 ± 0.065	0.398 ± 0.073	—	—	—
1998 KG_{62}	QB1/2	6.065 ± 0.078	23.450 ± 3.122	1.000 ± 0.060	0.561 ± 0.074	0.640 ± 0.040	—	—	—
1998 QM_{107}	Cent/1	10.226 ± 0.060	16.299 ± 3.246	0.730 ± 0.060	0.520 ± 0.030	—	—	—	—
1998 SG_{35}	Cent/2	10.828 ± 0.023	12.259 ± 2.768	0.725 ± 0.089	0.456 ± 0.050	0.546 ± 0.063	—	—	—
1998 SM_{165}	QB1/2	5.799 ± 0.190	33.103 ± 3.836	0.966 ± 0.091	0.687 ± 0.079	0.648 ± 0.073	—	—	—
1998 SN_{165}	QB1/4	5.736 ± 0.410	7.311 ± 4.410	0.712 ± 0.095	0.446 ± 0.089	0.419 ± 0.088	—	—	—
1998 TF_{35}	Cent/2	8.683 ± 0.193	34.880 ± 4.193	1.085 ± 0.111	0.697 ± 0.064	0.651 ± 0.119	—	—	—
1998 UR_{43}	Plut/3	8.090 ± 0.130	9.494 ± 5.465	0.784 ± 0.101	0.565 ± 0.106	0.268 ± 0.117	—	—	—
1998 VG_{44}	Plut/2	6.349 ± 0.057	24.105 ± 3.881	0.951 ± 0.055	0.567 ± 0.056	0.668 ± 0.116	—	—	—
1998 WH_{24}	QB1/7	4.512 ± 0.108	23.435 ± 3.338	0.924 ± 0.063	0.602 ± 0.043	0.547 ± 0.111	—	—	—
1998 WV_{24}	Plut/1	7.112 ± 0.040	14.117 ± 3.243	0.770 ± 0.010	0.500 ± 0.030	—	—	—	—
1998 WV_{31}	Plut/1	7.643 ± 0.070	10.197 ± 4.283	0.834 ± 0.089	0.513 ± 0.069	0.357 ± 0.114	—	—	—
1998 WX_{24}	QB1/1	6.232 ± 0.090	37.747 ± 5.234	1.090 ± 0.050	0.700 ± 0.050	—	—	—	—
1998 WX_{31}	QB1/1	6.225 ± 0.075	26.201 ± 4.606	—	0.602 ± 0.080	0.640 ± 0.112	—	—	—
1998 XY_{95}	Scat/1	6.492 ± 0.167	36.230 ± 7.184	0.939 ± 0.238	0.645 ± 0.140	0.772 ± 0.153	—	—	—
1999 CC_{158}	Scat/1	5.430 ± 0.074	20.293 ± 3.657	0.962 ± 0.098	0.571 ± 0.063	0.552 ± 0.088	—	—	—
1999 CD_{158}	QB1/1	4.903 ± 0.066	13.430 ± 3.734	0.871 ± 0.077	0.477 ± 0.065	0.543 ± 0.089	—	—	—

Table 1. Continued.

Object	(1)/(2)	M11 $\pm\sigma$	Grt $\pm\sigma$	$B-V\pm\sigma$	$V-R\pm\sigma$	$R-I\pm\sigma$	$I-J\pm\sigma$	$J-H\pm\sigma$	$H-K\pm\sigma$
1999 CF_{119}	Scat/1	7.031 ± 0.077	13.450 ± 4.603	—	0.557 ± 0.083	0.391 ± 0.107	—	—	—
1999 DE_{9}	Scat/2	4.804 ± 0.056	20.506 ± 2.281	0.915 ± 0.058	0.572 ± 0.042	0.559 ± 0.049	—	—	—
1999 HB_{12}	Scat/1	—	8.150 ± 3.096	0.870 ± 0.060	0.500 ± 0.050	0.320 ± 0.080	—	—	—
1999 HR_{11}	QB1/1	—	29.372 ± 4.428	0.920 ± 0.120	0.530 ± 0.100	0.800 ± 0.070	—	—	—
1999 HS_{11}	QB1/1	—	30.142 ± 4.784	1.010 ± 0.160	0.680 ± 0.100	0.600 ± 0.090	—	—	—
1999 KR_{16}	QB1/1	5.505 ± 0.020	44.581 ± 1.577	1.100 ± 0.050	0.740 ± 0.030	0.770 ± 0.030	—	—	—
1999 OX_{3}	Cent/3	7.272 ± 0.196	28.215 ± 3.746	1.072 ± 0.117	0.692 ± 0.055	0.475 ± 0.109	—	—	—
1999 OY_{3}	QB1/1	6.303 ± 0.040	0.952 ± 2.294	0.710 ± 0.010	0.370 ± 0.020	—	—	—	—
1999 RY_{215}	QB1/1	—	—	0.800 ± 0.100	—	0.780 ± 0.080	—	—	—
1999 RZ_{253}	QB1/2	5.428 ± 0.056	29.962 ± 3.002	0.820 ± 0.170	0.646 ± 0.058	0.647 ± 0.062	—	—	—
1999 TC_{36}	Plut/5	4.920 ± 0.070	32.331 ± 2.382	1.008 ± 0.050	0.687 ± 0.041	0.625 ± 0.056	—	—	—
1999 TD_{10}	Scat/2	8.706 ± 0.022	11.893 ± 1.908	0.770 ± 0.050	0.495 ± 0.040	0.470 ± 0.032	—	—	—
1999 TR_{11}	Plut/1	8.058 ± 0.140	44.369 ± 7.259	1.020 ± 0.080	0.750 ± 0.070	—	—	—	—
1999 UG_{5}	Cent/5	10.483 ± 0.134	25.886 ± 2.677	0.964 ± 0.085	0.607 ± 0.060	0.625 ± 0.042	—	—	—
2000 EB_{173}	Plut/17	4.657 ± 0.110	22.884 ± 3.969	0.954 ± 0.050	0.565 ± 0.090	0.623 ± 0.061	—	—	—
2000 OK_{67}	QB1/2	6.138 ± 0.063	15.972 ± 7.056	0.727 ± 0.108	0.517 ± 0.068	—	—	—	—
2000 PE_{30}	Scat/1	—	4.713 ± 2.049	0.710 ± 0.050	0.380 ± 0.040	0.450 ± 0.040	—	—	—
2000 QC_{243}	Cent/1	7.949 ± 0.049	6.961 ± 2.724	0.724 ± 0.062	0.448 ± 0.044	0.397 ± 0.069	—	—	—
2000 WR_{106}	QB1/1	3.048 ± 0.059	39.611 ± 3.536	1.017 ± 0.071	0.711 ± 0.071	0.730 ± 0.071	—	—	—

(1) Class: QB1 = Cubewano, Plut = Plutino, Cent = Centaur, SPC = Short Period Comet, LPC = Long Period Comet. (2) Number of epochs. Grt is the spectral gradient $\mathcal{S}$ (%/100 nm). M11 is the absolute R magnitude.

2. Dataset and general description of individual MBOSSes

2.1. Dataset – Average magnitudes and colors

In order to get the most significant results, the statistical analysis presented in this paper were based on a complete compilation of all the TNO and Centaur colors that have been reported in the "Distant EKO" web page (Parker 2001), as of 2001. Several additional papers, preprint and private communications about TNOs and Comets were also added. We realize that such a compilation can never be complete and up-to-date; the current database is frozen in its current state, and we plan to add new and missing papers in future versions. Refer to Appendix A for the references that were used for each object. Authors are encouraged to send us their measurements electronically (`ohainaut@eso.org`), so that we can include them in this database.

When available, the individual magnitudes were used, so that non-standard color indexes (i.e. not the traditional $B-V$, $V-R$...) can be computed (we hereby encourage the authors to publish these individual magnitudes). Where the magnitudes were not available, we used the published color indexes. In this compilation, no correction has been made for the different photometric systems used. Only the name of the filter is taken into account, so that $R_{\rm Bessel}=R_{\rm KC}$, $K=K'=Ks$, etc. We assume that the errors introduced by these assumptions are small compared to the measurement errors. As all the TNO measurements were obtained after 1992, a large fraction of them were calibrated using the standard stars by Landolt (1992). If the authors computed the color term of their system and applied them, the magnitude they published are de facto in the Bessel system as described by Landolt, further reducing possible color discrepancies between the different filter system used.

For a given epoch (loosely defined as "within a few hours"), we computed all the possible colors and magnitudes based on the available colors and magnitudes. It is important to note that no additional color indexes were computed at that stage (i.e. if V is available at one epoch, and R at another, the $V-R$ index is *not* computed mixing these epochs). Some publications list colors obtained by combining magnitudes obtained at different epochs. These were *not* entered in the database. We also checked for and removed multiple entries for the same measurements that appeared in different papers.

The magnitudes and colors from different epochs (and different authors) were combined in order to obtain one average magnitude and color set per object. However, no new color indexes are computed even if we now have enough data (e.g. if an author reported a $R-I$ and another $I-J$, we do not compute nor use the resulting $R-J$), as these would not be obtained from simultaneous data. In this way, even if the object presents some intrinsic magnitude variability, we do not introduce any additional color artifacts. The average magnitude that we publish here corresponds to the average of the (possibly varying) magnitudes, and the average colors is the average of the measured colors. The variations of magnitude will *not* contribute to the color error.

For this combination, $\bar{x}$, the average magnitude or color is obtained by weighted average of the individual magnitudes and colors. We did not a priori reject any published measurement, nor give a stronger or lighter weight to the measurements from a given author or team. We did not give a larger weight to measurements obtained on a larger telescope. For this study, we fully trust and rely on the published error bars: the weight of a measurement is set to $1/\sigma$:

$$\bar{x}=\frac{\sum_{i=1}^{N} x_i/\sigma_i}{\sum_{i=1}^{N} 1/\sigma_i}. \quad (1)$$

Using this weight, very good measurements (trusting their small σ) will be given a strong weight compared to approximate values. In case of multiple measurements $x_i, i=1...N$ of an item (magnitude or color), the error σ is computed as a combination of the individual errors σ_i and of

the dispersion of the measurements around their mean $\bar{x}$, using

$$\sigma = \sqrt{\frac{\sum_{i=1}^{N} \sigma_i}{\sum_{i=1}^{N} 1/\sigma_i} + \frac{\sum_{i=1}^{N} (x_i - \bar{x})^2/\sigma_i}{(N-1)\sum_{i=1}^{N} 1/\sigma_i}}. \quad (2)$$

The first term in the root corresponds to the increase of the Signal-to-Noise ratio resulting from the multiple measurements, while the second term is the variance of the measurements (the $N-1$ is because we don't have a priori knowledge of the mean). With this combination, a measurement with a large error will have a small contribution to the final average and error. On the other hand, two equally good measurements having different values will have a resulting error that is larger than the individual ones, reflecting a possible variation and a definite uncertainty on the value. In case only one measurement is available, it is reported with its error bar in the final table. Some objects were measured several times. The dispersion of these measurements is similar to the error bars, suggesting that no dramatic systematic effects affect the different teams, and therefore indicating that the combined data are of better quality than the individual ones. The averaging program also includes a warning system checking for very different values of given color of an object (the limit corresponds to an incompatibility at the 3σ level taking into account the sum of the considered error bars). The current database did not trigger this warning.

The classical color indexes are reported in Table 1. In this table, the un-named objects are identified by their temporary MPC designation (e.g. 1992 QB_1), while the named objects are identified with their number and name. For uniformity, we don't use the number of numbered but still un-named object. In the case of the numbered comets, their IAU designation is used.

The table also lists the number of independent epochs that were combined for each object.

2.2. Absolute magnitude

For each epoch, we attempted to compute an absolute R magnitude: for this purpose, we used either the measured R magnitude, when available, or another magnitude and the corresponding color index with R. The helio- and geo-centric distances (r and Δ, resp., [AU]) were computed using a two-body ephemerides program with the orbital elements available at MPC, and the absolute magnitude $M(1,1)$ was computed using

$$M(1,1) = R - 5\log(r\Delta). \quad (3)$$

Because *i*) the phase angle is usually small for MBOSS observations, *ii*) this angle does not change significantly from epoch to epoch, and *iii*) the phase function is unknown for most MBOSSes, we neglect the phase correction. Because of *i*) and *ii*), this correction would in any case not change significantly the result. The $M(1,1)$ for all available epochs were averaged using the same procedure as described above; the error was also computed.

Table 2. Solar colors used in this paper, from Hardorp (1980), Campins et al. (1985) and Allen's Astrophysical Quantities, Cox (2000).

Color	Value	Color	Value
$U-B$	0.204	$V-K$	1.486
$U-V$	0.845	$J-H$	0.23
$V-R$	0.36	$H-K$	0.06
$V-I$	0.69		

The results are also listed in Table 1. Assuming a value for the surface albedo p, these absolute magnitude can be converted into the radius R_N of the object [km] using the formula from Russell (1916)

$$pR_N^2 = 2.235 \times 10^{22} \times 10^{0.4(M_\odot - M(1,1))}, \quad (4)$$

where $M_\odot$ is the R magnitude of the Sun and $M(1,1)$ is the absolute R magnitude from Eq. (3). As the albedo p is not known (except for a couple of objects), and in particular because neutral-grey objects could either correspond to extremely old surfaces (with p as low as 0.02, Thompson et al. 1987) or to objects covered with fresh ice (therefore having a higher albedo, possibly as high as that of Pluto, 0.3, or Chiron, 0.1), we do not give a generic conversion of $M(1,1)$ into a radius.

2.3. Spectral gradient

The information contained in the color indexes can be converted into a very low resolution reflectivity spectrum $\mathcal{R}(\lambda)$ (Jewitt & Meech 1986), using

$$\mathcal{R}(\lambda) = 10^{-0.4(m(\lambda) - m_\odot(\lambda))}, \quad (5)$$

where m and $m_\odot$ are the magnitude of the object and of the Sun at the considered wavelength. Normalizing the reflectivity to 1 at a given wavelength (in our case, the V central wavelength), we have

$$\mathcal{R}(\lambda) = 10^{-0.4((m(\lambda)-m(V))-(m(\lambda)-m(V))_\odot)}. \quad (6)$$

The solar colors used are listed in Table 2. The reflectivity spectra are given in Fig. 1.

Boehnhardt et al. (2001) have compared such magnitude-based reflectivity spectra with real spectra (i.e. obtained with a spectrograph) for ∼10 objects observed quasi-simultaneously with a large telescope (one of ESO's 8 m VLTs) through broad-band filters and with a low resolution spectrograph. He found a excellent agreement between real and magnitude-based spectra.

We can introduce a description of the reflectivity spectrum: the reddening $\mathcal{S}$, also called slope parameter or spectral index, which is expressed in percent of reddening per 100 nm:

$$\mathcal{S}(\lambda_1, \lambda_2) = 100.\frac{\mathcal{R}(\lambda_2) - \mathcal{R}(\lambda_1)}{(\lambda_2 - \lambda_1)/100}. \quad (7)$$

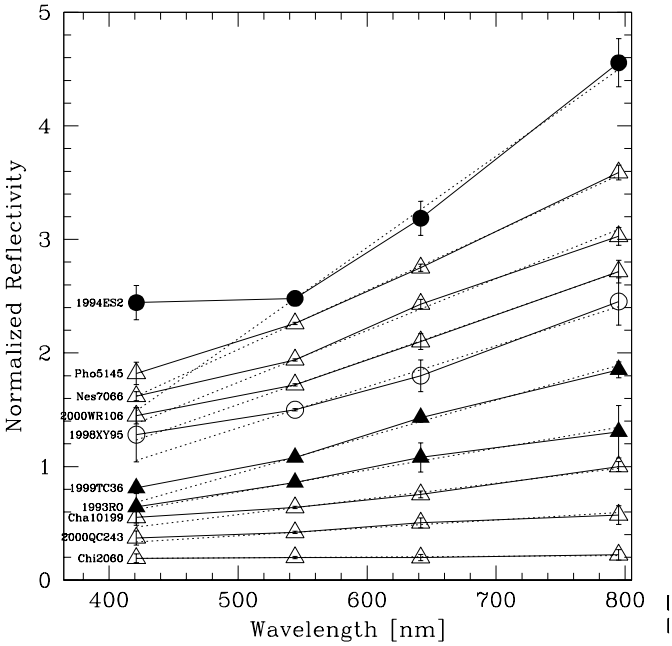

Fig. 1. Examples of reflectivity spectra, sorted by increasing gradient. The reflectivity is normalized to 1 for the V filter; the spectra have been arbitrarily shifted for clarity. For each object, the dotted line is the linear regression over the V, R, I range, corresponding to the gradient $\mathcal{S}$. Similar reflectivity spectra are available for all the objects of the database on our MBOSS web site.

Boehnhardt et al. (2001) realized that all the objects observed with a high S/N display a *linear* reflectivity spectrum over the $V-R-I$ range. We can therefore introduce a global value for $\mathcal{S}$, describing the spectrum over the $V-R-I$ range. We obtained the value of $\mathcal{S}$, together with its uncertainty, by linear regression of $\mathcal{R}$ as given in Eq. (6). We restricted this fit to the objects having at least two color indexes measured. The values of $\mathcal{S}$ and its error are listed in Table 3. We also restricted the fit to the V, R and I filters, excluding B, because the B reflectivity shows a systematic trend, as described below. The error on $\mathcal{S}$ is a combination of the error on each $\mathcal{R}(\lambda)$ (obtained by propagation of the errors on the colors) and on the linear regression. In order to further characterize the shape of the spectrum, we introduced d, the total deviation of the reflectivity with respect to the linear regression:

$$d = \sum_{\lambda=B,V,R,I} (\mathcal{R}(\lambda) - \mathcal{R}_l(\lambda)), \quad (8)$$

where $\mathcal{R}_l$ is the reflectivity expected from the linear fit. Positive values of d correspond to spectra with a global concavity, while negative values correspond to a convexity. The concavity d can be interpreted in two ways: either *i)* one considers that the result published by Boehnhardt et al. (2001) can be generalized to all MBOSSes; in that case, objects with a large $|d|$ suffer from large uncertainties and should be re-measured with a better S/N, or *ii)* it is considered as real, and large values of $|d|$ denote objects whose spectral characteristic are intrinsically different and worth a more detailed study. In both cases, observers should take a closer look at the objects identified by a large deviation $|d|$ in Table 3. These objects are (7066) Nessus, 1991 QB_1, 1993 SC, 1994 ES_2, 1994 TB, 1996 RR_{20} and 1999 KR_{16}.

Table 3. Reddening Index $\mathcal{S}$ and its error, and deviation d from a linear spectrum for the objects in the database, available electronically at `http://www.edpsciences.org`.

It is interesting to note that the coordinates $(\mathcal{S}, d)$ of an object are very similar to the "principal components" (PC1,PC2) that Barucci et al. (2001) have obtained from an analysis of the colors of 22 objects: the position of a MBOSS in a multi-dimensional color diagram is determined primarily by PC1 (which can physically be associated to $\mathcal{S}$) and to a much lesser extent by PC2 (which would be related to d). The additional dimension of the multi-dimensional color diagram contain little information. We intent to apply a similar analysis to this dataset.

2.4. Color-color diagrams

Figure 2 shows a selection of color-color diagrams; the whole collection, for all possible color indexes, is available on the MBOSS web site. To guide the eye, the reddening line is drawn on each diagram. This line is constructed computing the colors for an object of a given reddening $\mathcal{S}$ using Eq. (7), and then connecting all the points for $-10 < \mathcal{S} < +70\%/100$ nm (a tick is placed every 10%). An object located directly on this line has a perfectly linear reflectivity spectrum, and its slope $\mathcal{S}$ can be estimated using the tick-marks on the line. Objects above the line have a concave spectrum (positive d), while objects below the line have a convex spectrum (negative d) over the spectral range considered.

As it was noted in Sect. 1.2, the three physical processes that are suspected to effect the color of a MBOSS surface independently produce linear reflectivity spectra (in first approximation, over the visible wavelength range). The average over the complete surface of an object will therefore also be a linear spectrum. Within that hypothesis, if no other physical processes plays an important role, and if the MBOSSes have the same original intrinsic composition, the objects should all lie on the reddening line. A young-surfaced object would have solar-like colors, and the aging will move the object up the reddening line, while collision and activity will move it back down. Similarly, an object left undisturbed long enough would evolve moving up the reddening line till it reaches the maximum possible reddening, then, the continued irradiation of its surface would cause it to further darken (Thompson et al. 1987), possibly moving back down on the reddening line. In that case, one could expect to find among the neutral objects some MBOSSes covered with fresh ice, together with objects with ancient ice, with a very dark albedo. This is tested later (cf. Sect. 3.4).

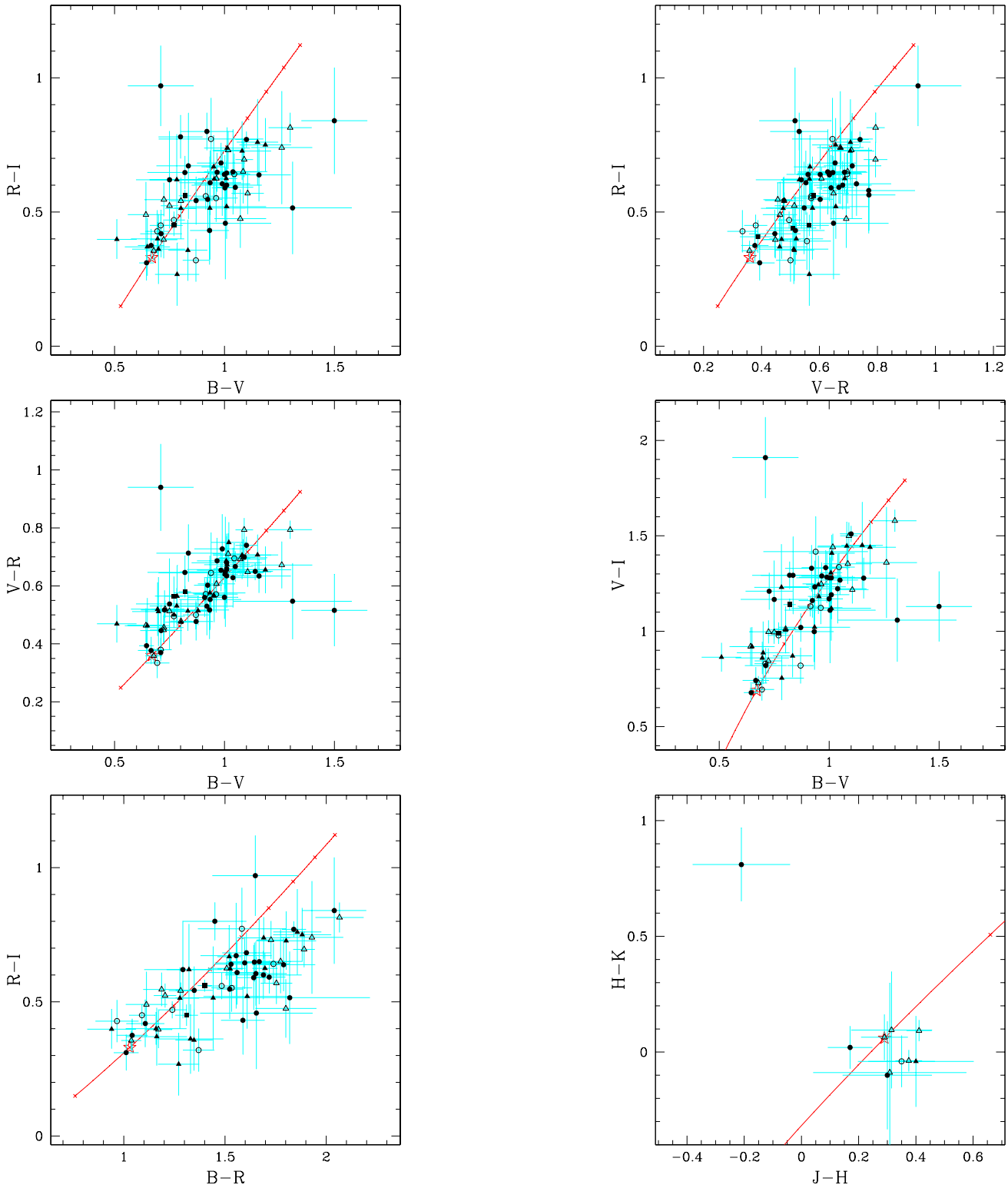

Fig. 2. MBOSS color-color diagrams. The meaning of the different symbols is given in Fig. 4. The reddening line ranges gradients from −10 to 70%/100 nm; a tick mark is placed every 10 units. The outliers objects in the $B-V$, $R-I$ are 1994 ES_2 (top left), 1994 EV_3 (top right), 1998 HK_{151} (bottom left), and 1995 DA_2 (middle right). All other combinations of colors are available on the MBOSS web site.

The diagrams from Fig. 2 are in agreement with this simple interpretation of the reddening line: the MBOSSes are clustered along that line. For the $(B-V)$ and $(V-R)$ colors, the deviations from the line are compatible with the error bars of the individual points, indicating that the spectra are linear over this wavelength range. The plots involving the $(R-I)$ color, however, show a systematic deviation from the line for the reddest objects (particularly

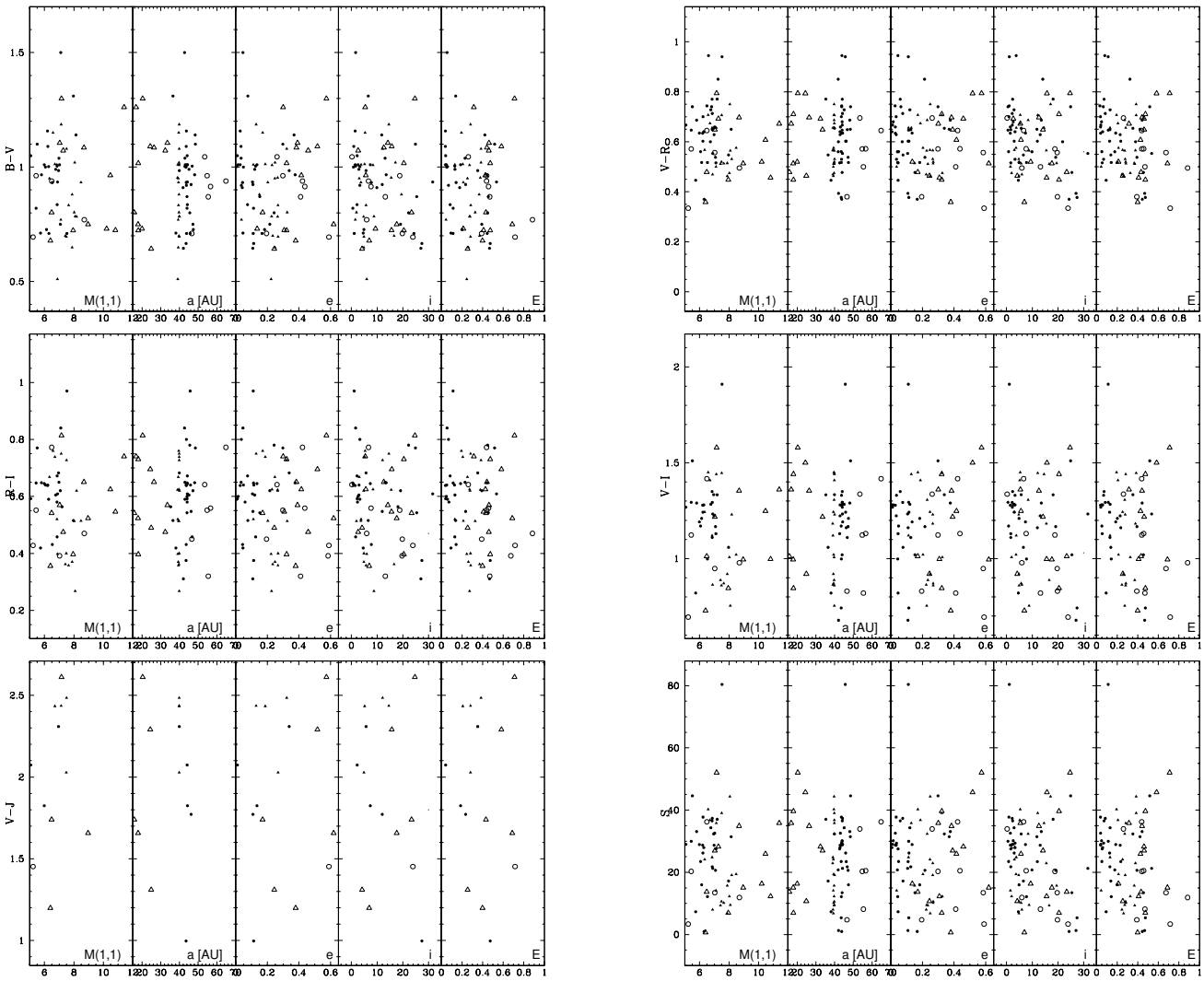

Fig. 3. Visible color distributions as functions of the absolute magnitude $M(1,1)$, the orbit semi-major axis a [AU], the eccentricity e, the inclination i and the orbit excitation $\mathcal{E}$ (see text for definition). The meaning of the different symbols is given in Fig. 4. Other colors are available electronically and on line at the MBOSS web site.

visible in the $(B-R)$ vs. $(R-I)$ diagram). This corresponds to the fact that the spectrum of the reddest objects flattens toward the IR, where it is typically flat/neutral (Davies 2000; McBride et al. 1999). One also notes a systematic deviation from the reddening line of the neutral to neutral-red points in the $B-V$ vs. $V-R$ diagram: the bulk of these points are significantly above the line; this corresponds to the bend observed around the B wavelength in many reflection spectra from Fig. 1. This bend is not observed in the "fresh ice" laboratory spectra published by Thompson et al. (1987), suggesting that in spite of their low reddening, the surface of these objects could be significantly processed.

It is also interesting to note a small group of 5 objects clustered very near the solar colors in the $B-V$ vs. $V-R$ diagram, i.e. in the range corresponding to fresh ice surface. Two of these objects are either known or suspected to be cometary active, i.e. (2060) Chiron (Tholen et al. 1988; Meech & Belton 1989) and 1996 TO_{66} (Hainaut et al. 2000). A detailed study of the others (1995 SM_{55}, 1996 TL_{66} and 1999 OY_3) is well deserved.

In addition to the simple "reddening line", it would be interesting to produce an evolution track of the color of laboratory ices, for increasing irradiation doses. Such work will be presented in another paper by the same authors.

The diagrams show notable outliers (i.e. isolated points, far from the reddening line and the general cluster of objects):

- 1994 ES_2, which has only one fairly old set of color measurements;
- 1994 EV_3, whose $V-R$ index is well established (and reasonable); other colors have only one measurement available;
- 1998 HK_{151}, whose $B-V$ has only one fairly old measurement while other colors are well established, and
- 1995 DA_2, whose B measurements is also fairly old;
- 1996 TO_{66} is an outlier only in the IR color diagram.

For all these objects, it seems that less accurate magnitudes from the early years of TNO photometry (before the VLT/Keck era) are the reason of the strange colors. We therefore encourage observers to acquire new colors for these objects. For instance, preliminary measurements of VLT data for 1994 ES_2 and 1994 EV_3 (Delsanti, priv. comm.) put these objects back in the main group.

3. Correlation with orbital parameters and size

In this section, we search for correlation between the color or reddening distributions and the orbital parameters, i.e. a, the semi-major axis, e, the eccentricity and i, the inclination. We also consider the "excitation" $\mathcal{E}$ of an object's orbit, defined as

$$\mathcal{E} = \sqrt{e^2 + \sin^2(i)}, \tag{9}$$

$\sin(i)$ is related to the object's velocity perpendicular to the ecliptic, and e to its radial velocity. Therefore, $\mathcal{E}$ is an estimate of the velocity of the object with respect to another object that would be at the same distance on a circular ecliptic orbit, it is therefore also related to the probability of collision, as well as the velocity of the impacts. The color vs. $\mathcal{E}$ plots therefore explore possible effect of collisions. The colors are also plotted as functions of $M(1,1)$, the absolute magnitude (cf. Sect. 2.2 and Eq. (3)).

3.1. Plots

Figure 3 displays some of the color indexes and the reddening slope $\mathcal{S}$ as a function of the orbital parameters and absolute magnitude. In each figure, each object is represented using the symbol of its class (cf. Fig. 2). The complete set of diagrams is available on the MBOSS web site; only some examples are reproduced here.

Results:

- a plots: the extreme redness of objects with $a > 40$ AU reported by Tegler & Romanishin (2000) is supported by the appearance of the $B - V$.
- No striking bimodality appears in any of the plots.
- None of the plot do show any convincing trend. In particular, the $V - J$ vs. $M(1,1)$ plot does not show any convincing trend: we do not confirm the correlation that Jewitt & Luu (1998) had observed on only 5 objects.

3.2. Correlation

In order to quantify possible correlations between the colors (and gradient) and the various orbital elements and absolute magnitude, we computed the correlation coefficient for each "Color" versus "orbital element" distribution. The test itself is described in Appendix B. As a reminder, while the correlation coefficient indicates how strong the correlation is (large absolute values), there is no way to quantify the significance of that correlation. The correlation coefficients were computed for the complete MBOSS population (i.e. *all* objects) and for the Plutinos, Cubewanos and Centaurs/Scattered objects separately. The numerical results of the tests are listed in Table C.1.

Results:

- For the complete MBOSS population: the colors and gradient are not correlated with any of a, e, i, $\mathcal{E}$ nor $M(1,1)$ (i.e. all the correlation coefficients are extremely low in absolute value).
- i, e, $\mathcal{E}$: for the Cubewanos, there is a systematic anti-correlation between the colors (and gradient) and the e, i and $\mathcal{E}$ parameters (i.e. objects with higher orbital excitation being bluer). This effect is visible for all colors, and is the strongest for the $B - R$ index. This effect completely disappears for the Centaurs/Scattered TNOs (coefficients close to zero). In the case of the Plutinos, the colors present a weak anti-correlation with the eccentricity (up to -0.2), and a weak correlation with the inclination ($\sim$0.2), both effects canceling each-other for $\mathcal{E}$.
- $M(1,1)$: for the Cubewanos, there is a correlation between the colors and the absolute magnitude, indicating that the objects with fainter $M(1,1)$ are redder. This effect is completely nonexistent for the Centaurs/Scattered TNOs, but appears reversed (i.e. bright $M(1,1)$ redder) for the Plutinos, with slightly weaker correlations.

3.3. Are there some more subtle effects

In order to test for more subtle effects than a simple correlation between the colors (or gradient) and the orbital elements (and $M(1,1)$), each population is divided in two sub-samples, i.e. the object having the considered element smaller than a given value, and those having that element larger. The boundary value is chosen as the median of the sample, i.e. to split the population in sub-samples of similar sizes. The median value is probably not the best choice on physical bases, but a physically better choice might lead to samples of fairly different sizes, which could cause asymmetry artifacts. The cut-off values are listed in Table C.1 with the results of the test described below.

The two samples are then compared using Student's t-test and f-test, which are described in Appendix B. In summary, small values of the probability associated to the t-test, indicate that both sub-populations have significantly different mean of the considered color (*Prob* is the probability that both subsumes are randomly drawn from a similar population), while small values of the probability associated to the f-test reveal that the sub-samples have different variances. Each test was performed on the whole MBOSS population and on the Plutinos and Cubewanos only. The numeric results of the tests and the cut values are listed in Appendix, in Table C.1.

Results: *t*-test

- For the complete MBOSS population as well as for the individual families, the t-test does not reveal any significant trend with respect to the semi-major axis a.
- The t-test applied to the color distribution vs. i, e and $\mathcal{E}$ reveals a strong, highly significant trend for the Cubewanos: objects with higher orbital excitations are bluer. The effect is systematic in all colors (and gradient), and its significance is in the $Prob = 10^{-3}$ range. This support the result presented by Trujillo et al. (2001) (i.e. a correlation between color and eccentricity, supported by similar t-tests) on a smaller sample. They interpreted this as an evidence that low $\mathcal{E}$ objects are less affected by (collisional) re-surfacing than objects with a high excitation (because the collisions are on average less violent, and/or less numerous). Stern (oral communication at the Meudon 2001 meeting) also mentioned the correlation with $\mathcal{E}$.
- This effect completely vanishes for the Plutinos and Centaurs/Scattered TNOs: the various sub-samples are statistically equivalent. It appears diluted when considering all MBOSSes together.
- Considering the Plutinos colors as a function of their absolute magnitude, a marginally significant trend appears, indicating that those with a fainter $M(1,1)$ are slightly bluer. For the Cubewanos, the opposite trend exists: those with a fainter $M(1,1)$ are slightly redder. It is also worth noting that the median $M(1,1)$ (used as cut-off between the sub-samples) is fainter for the Plutinos (7.4) than for the Cubewanos (6.6). This is a natural discovery selection effect: as the Plutinos are on average at smaller heliocentric distances than the Cubewanos, smaller objects can be discovered. As a consequence, the test on the Plutinos explores intrinsically smaller objects. Setting the cut-off magnitude for the Plutinos equal to that of the Cubewanos produces unbalanced samples, but the result remains the same.

Results: *f*-test

- The color distributions of objects as a function of the absolute magnitude: in earlier versions of this database, the $B-*$ and $*-I$ ($*$ indicating any other filter) of objects with fainter $M(1,1)$ had significantly broader color distributions than the objects with brighter absolute magnitudes. This was tracked down to an instrumental effect: the B and I magnitudes are typically affected by larger error bars because of the lower quantum efficiency of the detectors in these bands. Objects with fainter absolute magnitude are on average fainter than those with a brighter $M(1,1)$, and therefore have larger error bars. Recent addition to the database of a large number of observations obtained with 8–10 m-class telescopes diluted that effect out. In the current version of the database, the MBOSSes with faint $M(1,1)$ (i.e. probably the smaller ones) do not present a significantly different color distribution width than the bright ones. This is true for the MBOSSes as a whole and for the different classes. This is contrary to the predictions of a collisional resurfacing model (Luu & Jewitt 1996a; Jewitt & Luu 2001).
- Cubewanos with higher orbital excitation (i.e. larger i, e and/or $\mathcal{E}$) have significantly broader color distributions than the others. The effect is strongly significant except for $B-V$ and $*-I$, where the effect is partially diluted by larger error bars on B and I magnitudes. For the Plutinos and Centaurs/Scattered TNOs, the effect disappears, except for the inclination (but it is not significant).

3.4. Broadening of the $M(1,1)$ distributions?

As mentioned earlier, neutral-bluish objects could have their surface covered with fresh ice (resulting from a recent re-surfacing), or, on the contrary, with extremely ancient, extremely irradiated ice (with doses of 10^{10} erg cm^{-2}), whose color is also expected to be neutral (cf. laboratory spectra published by Thompson et al. 1987). The albedo of the ancient ice is expected to be significantly lower than that of the fresh ice. On the other hand, very red objects are expected to be covered with highly irradiated ice (corresponding to the laboratory samples that received doses of 10^9 erg cm^{-2} Thompson et al. 1987), and would have a much narrower range of albedo. If we assume that all these objects have a similar radius distribution, the resulting $M(1,1)$ distribution should be significantly broader for the neutral objects than for the red ones (cf. Eq. (4)).

In order to test this hypothesis, we consider the $M(1,1)$ distribution as function of the colors (i.e. the reverse of the previous section). We split the observed sample in two, i.e. those with colors redder than a limit, and the others. The cut-off value is set at the mid-point between the minimum and maximum values of the considered color. The average values of $M(1,1)$ and their variances are computed for each sub-samples, and are compared using the f-test (cf. Sect. B), which evaluates whether the two variances are compatible. This test was performed for all the colors and the gradient distributions, for the complete MBOSS population, and for the Plutinos, Cubewanos and Centaurs/Scattered TNOs only. The numerical results of these tests are listed in Table C.2.

Results:

- Restricting the test to the Plutinos, it appears that the redder objects have a broader $M(1,1)$ distribution (strongly significant effect) than the bluer ones. This effect is visible and significant (<1%) in all color indexes.
- This effect is also visible for the Centaurs/Scattered TNOs (redder objects have a broader $M(1,1)$

Table 4. Average colors of the various classes of objects. For each color, the table lists the number of objects included in the statistics, as well as the average color and the square root of the corresponding variance (which is undefined and set to 0 in case only one object is available).

Color	Plutinos		Cubewanos		Centaurs		Scattered		Comets	
$U-B$	0	— —	1	1.000 ± 0.000	0	— —	1	0.970 ± 0.000	0	— —
$U-V$	0	— —	1	1.720 ± 0.000	0	— —	1	1.710 ± 0.000	0	— —
$U-R$	0	— —	1	2.120 ± 0.000	0	— —	1	2.150 ± 0.000	0	— —
$U-I$	0	— —	1	2.500 ± 0.000	0	— —	1	2.410 ± 0.000	0	— —
$B-V$	20	**0.886 ± 0.176**	33	**0.946 ± 0.185**	15	**0.930 ± 0.219**	8	**0.863 ± 0.126**	2	0.795 ± 0.035
$B-R$	20	**1.464 ± 0.261**	30	**1.561 ± 0.249**	15	**1.513 ± 0.349**	8	**1.376 ± 0.262**	2	1.355 ± 0.064
$B-I$	17	**1.977 ± 0.412**	25	**2.131 ± 0.329**	14	**2.119 ± 0.489**	7	**1.914 ± 0.412**	2	1.860 ± 0.141
$B-J$	0	— —	0	— —	5	2.800 ± 0.807	0	— —	0	— —
$B-H$	0	— —	0	— —	4	3.395 ± 0.679	0	— —	0	— —
$B-K$	0	— —	0	— —	4	3.428 ± 0.623	0	— —	0	— —
$V-R$	20	**0.580 ± 0.091**	40	**0.629 ± 0.132**	15	**0.590 ± 0.136**	9	**0.528 ± 0.116**	13	**0.430 ± 0.140**
$V-I$	17	**1.118 ± 0.239**	30	**1.206 ± 0.225**	13	**1.169 ± 0.270**	9	**1.031 ± 0.242**	4	0.964 ± 0.136
$V-J$	4	2.345 ± 0.213	5	1.795 ± 0.495	6	**1.801 ± 0.552**	1	1.452 ± 0.000	0	— —
$V-H$	0	— —	0	— —	5	2.245 ± 0.555	0	— —	0	— —
$V-K$	0	— —	0	— —	5	2.299 ± 0.506	0	— —	0	— —
$R-I$	17	**0.542 ± 0.161**	30	**0.613 ± 0.137**	14	**0.582 ± 0.134**	9	**0.509 ± 0.138**	4	0.465 ± 0.066
$R-J$	0	— —	0	— —	6	**1.243 ± 0.382**	0	— —	0	— —
$R-H$	0	— —	0	— —	5	1.658 ± 0.400	0	— —	0	— —
$R-K$	0	— —	0	— —	5	1.695 ± 0.367	0	— —	0	— —
$I-J$	0	— —	0	— —	6	**0.685 ± 0.233**	0	— —	0	— —
$I-H$	0	— —	0	— —	5	1.087 ± 0.234	0	— —	0	— —
$I-K$	0	— —	0	— —	5	1.124 ± 0.209	0	— —	0	— —
$J-H$	2	0.800 ± 0.566	4	0.228 ± 0.355	5	0.340 ± 0.051	1	0.350 ± 0.000	0	— —
$J-K$	1	0.360 ± 0.000	3	0.330 ± 0.234	5	0.383 ± 0.076	1	0.310 ± 0.000	0	— —
$H-K$	1	−0.040 ± 0.000	3	0.243 ± 0.494	5	0.025 ± 0.083	1	−0.040 ± 0.000	0	— —
Grt (%/100 nm)	20	**21.760 ± 12.305**	35	**26.537 ± 14.100**	15	**24.316 ± 15.086**	9	**16.948 ± 11.906**	4	12.894 ± 7.192

distribution) but although it is visible in all indexes, it is not statistically significant.
- The reversed effect (bluer objects have a broader $M(1,1)$ distribution) for the Cubewanos. The significance is not as strong as for the Plutinos, but still to be considered (all of the indexes are at the ∼5–6% level or stronger).
- No effect is visible for the MBOSSes as a whole.

Combining this with the results of correlations (Sect. 3.2), it implies that the objects with a bighter $M(1,1)$, i.e. the redder Plutinos and the bluer Cubewanos, cover a broader $M(1,1)$ range than the fainter ones. This is an effect of the steep luminosity function: there are much fewer objects per unit magnitude brighter than the cut-off magnitude (therefore the sample covers a broad range of M), while the number of objects per unit magnitude is much larger for those fainter than the cut-off. As the samples have roughly the same size, the faint ones cover a smaller magnitude range than the bright ones.

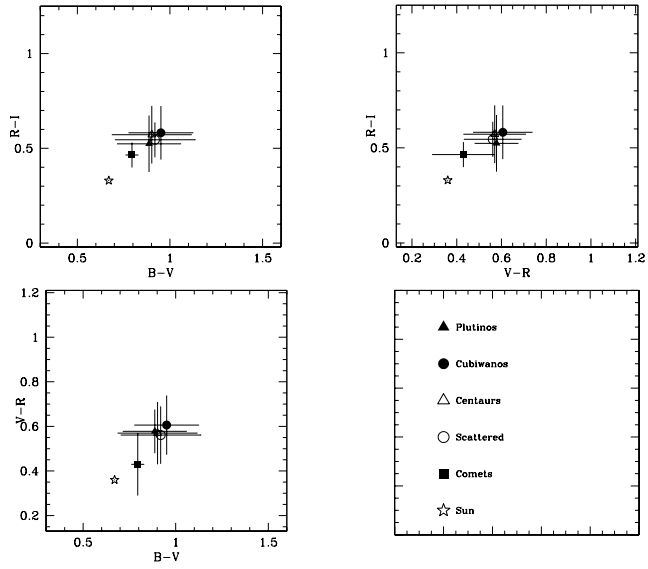

Fig. 4. Color-color diagrams of the average populations

4. Individual populations

4.1. Average and Variances

For each class of MBOSS, we compute the average color indexes. Table 4 lists the average colors of the various classes of objects together with the square root of their variances (which will become equivalent to the standard deviation for large samples with a ∼normal distribution). These values are of practical interest, for instance when preparing observations of an object whose colors are not known.

Figure 4 displays the average populations' colors in a set of color-color diagrams.

4.2. Histograms and cumulative probability functions

It is customary to visually compare distributions of objects using their histograms, i.e. the number of objects if given bins. Such histograms are displayed in Fig. 5. However, one has to be extremely careful in working with such plots: the size of the bin has a strong influence on the shape of the final histogram. Indeed, binning the data is equivalent to smoothing the data with a window equal

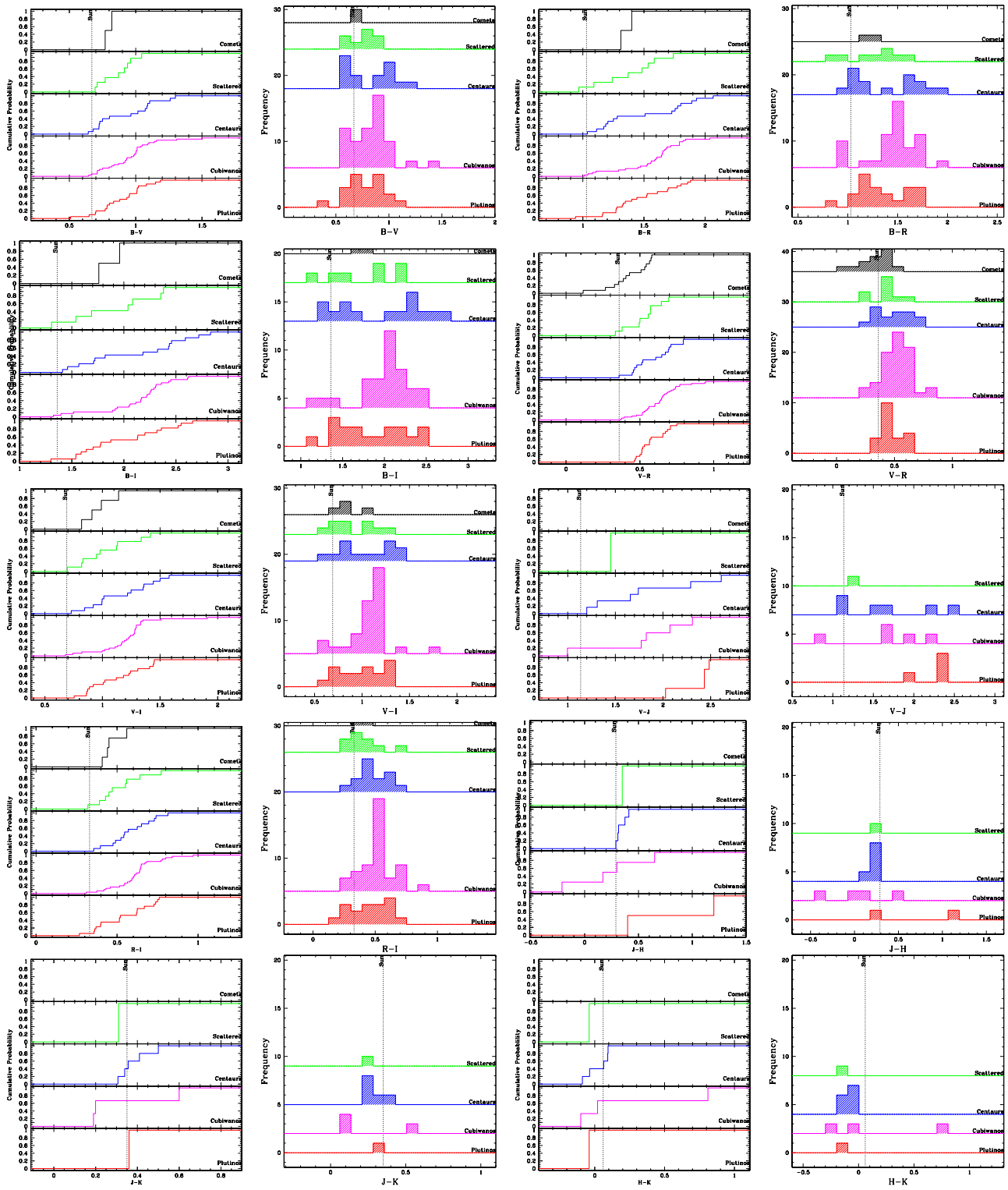

Fig. 5. CPF and histograms for the color indexes for all the classes of object.

to the bin size. Structures in the distribution that have a size similar to or smaller than the bin will be masked in the histogram, an effect that can create dangerously convincing – but wrong – artifacts.

A better way to represent a distribution is its Cumulative Probability Function (CPF). If one of the sample is $x_1, x_2, ..., x_n$ (e.g. the $V - R$ color indexes of n Centaurs), the corresponding CPF $F(x)$ is the fraction of the sample whose value is smaller than x. The CPF always has a typical "S" shape, with $F(-\infty) = 0$, and F increases by step at each x_i till it reaches a value of 1 when x is larger than all the x_i. The advantage of the CPF is that no information is lost with respect to the original distribution. While its use is not as instinctive as that of

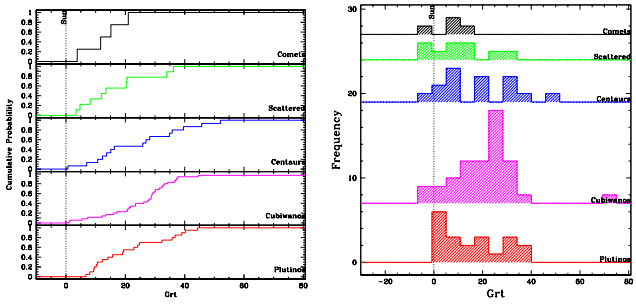

Fig. 5. Continued. CPF and histograms for the Gradient $\mathcal{S}$.

the histogram, it is a worthwhile exercise to train ones eye to use them. The CPFs are also displayed in Fig. 5

5. Population comparisons

5.1. Using the CPFs

The eye is extremely good at finding patterns and comparing shapes. In this first paragraph, we shall analyze visually the color histograms and CPFs. Of course, this analysis is only qualitative, and no claim is made with respect to the significance of these descriptions. They are meant to attract the attention of the reader to features that might eventually become significant – or may disappear when more data become available. In the next section, we will reconsider these comparisons with the cold (and less imaginative) eye of statistical tests.

Results

- Shift: apart from the comet $V-R$ that appears to be on average bluer than that of the other objects, no systematic difference of color is apparent;
- Broadening: defining the width of a color distribution by the interval over which the CPF is strictly between 0 and 1 (excluded), no class is systematically the broadest of all (the broadest is always either the Cubewanos or the Centaurs). The population with the narrowest color distribution is in almost all cases the Scattered TNOs;
- Several distributions show some discontinuities; in particular the Cubewanos and Centaurs' $B-V$, $B-R$ and $B-I$ as well as the Cubewanos' $V-I$ display a broken CPF, with first a sharp then a shallower increases (corresponding to a narrow then a broad peak in the histograms). Other distributions are very smooth with a constant increase rate, such as the Plutinos' $B-V$, $B-R$, $B-I$, $V-I$ and $R-I$.

5.2. Statistical tests

In this section, we will apply statistic tools to the available dataset in order to cast some light on the question of similarities and differences between the different classes of objects.

The problem at hand is to compare samples of 1D continuous distributions (colors, e.g. $V-R$), in order to decide whether they are statistically compatible. We will consider the MBOSS classes two by two. For that purpose, we shall use the t-test, the f-test, and the Kolmogorov-Smirnov (KS) test, which are described in more detail in Appendix B; each of them produce a probability *Prob*. Low values of *Prob* indicate that the distributions are statistically incompatible, but larger values can only be interpreted as stating that the distributions are not incompatible, *not* that they are equal; this is also discussed in more details in Appendix B.

In order to get a known comparison when studying the real MBOSS populations, we introduced two pairs of artificial subsets of the objects. They are defined as following:

- Odd: objects with odd numbers in the internal database;
- Even: objects with even numbers in the internal database;
- 1999: objects discovered in 1999, and
- non-99: objects not discovered in 1999.

Odd and Even are two populations of about the same size, while 1999 is much smaller than non-99. As the members of these populations are chosen using non-physical properties from the whole sample, we expect them to be equivalent, and that the statistical tests will give large values of *Prob* when comparing them. We performed all the tests on the "Odd/Even" and "1999/non-99" pairs, and report the results together with the tests on real classes. This allows the reader to get an idea of the statistical tests' calibration. 1999 was chosen as opposed to earlier years, because of the fairly large number of objects in the database (19) and because in that year the survey techniques were already quite advanced; in that way, we should not have a bias against small objects, that would have been present for the earlier years.

5.2.1. t-test: Are the mean colors compatible?

Table 4 lists the mean colors of the different classes. The color of an object is function of the nature of its surface and of the reddening and resurfacing it experienced. For a given population, the mean color will therefore give an information on the equilibrium reached between the aging reddening and the different re-surfacing processes.

The question we address in this section is whether the mean color of different classes are significantly different. The traditional way to compare the means of distributions is to use Student's t test; the implementation used for this work is described in Appendix B.2.1. The values of t and *Prob* are listed in Table C.3; the results for the artificial classes are displayed in Table C.4.

Results

- The 1999/non-1999 test classes do not show incompatibilities at the 9–10% level, except for very small

samples, indicating that one should consider these levels with suspicion when comparing small samples;
– The mean $V-R$ of the Comets is incompatible with those of the Cubewanos (with a significance of 10^{-3}), of the Plutinos, and the Centaurs, and marginally incompatible with those of the Scattered TNOs. This validates the visual impression that one has looking at the CPFs: the Comets are significantly bluer than the other objects;
– There is no significant incompatibility between the Plutinos, Cubewanos and Centaurs. Although the low- and high orbital excitation Cubewanos have incompatible color distributions, once considered all together, are indistinguishable (with the t-test) from the other classes.

5.2.2. f-test: Are the variances compatible?

The variance of the color distribution contains some information on the diversity of the population, and on the range covered by the reddening and resurfacing processes. For instance, one could expect that – although reaching a different mean equilibrium – the aging, the collisions and the cometary activity broaden the color distribution in a similar way, ranging from bluish, fresh ice, to deep red, undisturbed, aged surface.

In this section, we will determine whether the variances of the color distributions are significantly different (independently of their mean, that can be either similar or different). This is quantified using the f-test, described in Appendix B.2.2. The values of F and $Prob$ are listed in Table C.5.

Results:

– None of the variances show incompatibilities with a high level of significance.

The f-test does not give any significance to the fact that the color distributions of the Scattered TNOs cover systematically a narrower range than that of the other classes. This can be either because it *is* not significant, but also because the distributions have fairly different shapes.

5.2.3. KS test: Are the distributions compatible?

Obviously, the whole information from a distribution is not contained in its two first moments (mean and variance). A more complete comparison of the color distributions is therefore interesting. The ideal statistics tool for this purpose is the KS test (described in Appendix B.2.3), in which the two samples are compared through their complete Cumulative Probability Function (CPF). The values of d and the associated probability $Prob$ are listed in Table C.6 for the real classes of objects. Those for the test classes are available only electronically.

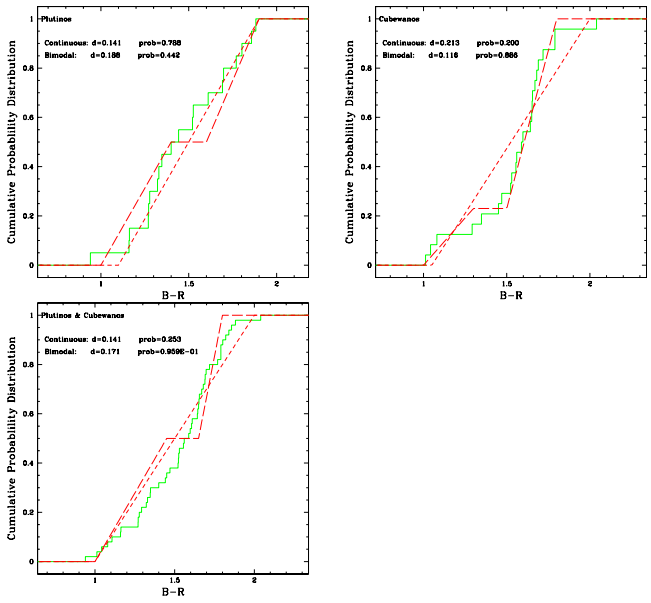

Fig. 6. Examples of CPF of the TNO color distributions, compared with the CPF of bimodal and continuous model distributions. The model distributions have been adjusted for a match of the observed distribution.

Results:

– The Comets' $V-R$ are incompatible (10^{-2}–10^{-3}) with the Cubewanos, Plutinos and Centaurs, but the incompatibility with the scattered TNOs that was noticed with the t-test is not apparent here;
– The other classes do not present significant incompatibilities.

6. Distribution bimodality

In this section, we will tackle the question of the bimodality of the TNO color distributions. Tegler and Romanishin have repeatedly reported that their observations lead to a classification of the objects in 2 separate groups in the color-color diagrams (Tegler & Romanishin 1998; Tegler & Romanishin 2000), one being of neutral-blue colors, while the other is very red. While this bimodality appears evident to the eye on their color-color diagrams, other authors (Barucci et al. 2000; Davies 2000; Delsanti et al. 2001) do not confirm it: their color-color diagrams show continuous distributions. Is Tegler and Romanishin's bimodality a selection artifact, or is it real? Since their original report, they have refined their claim, indicating that the bimodality affects only the most distant MBOSSes, i.e. the Cubewanos (Tegler & Romanishin 2000).

One of the reason invoked by Tegler and Romanishin to explain that they see this bi-modality while others don't, is that their own photometry is more accurate than that of other groups. While it is true that measuring faint MBOSSes is tricky, this claim cannot be valid anymore: i) many measurements (by other groups) have been performed on VLT-class telescopes, ensuring very good S/N ratios, and ii) the measurements presented in

Table 5. 1D color distribution models and corresponding KS statistics for various color indexes. The first column indicates which population is taken into consideration (Plutinos, Cubewanos or both), the second gives the color distribution used. The parameters listed corresponds to the best fitting models. The table is available in electronic form at `http://www.edpsciences.org`.

this compilation are often combining the result of various groups (a few objects combine >10 different measurements, many >5). The small resulting errors (which takes into account the dispersion between these measurements) indicate that the dispersion is rather small.

We will now compare the observed color distributions to simple models – continuous and bimodal ones, and try to decide whether the data are incompatible with one or the other. We will first consider the 1D distributions (e.g. $B-V$), then 2D distributions, corresponding to color-color diagrams.

6.1. 1D distributions

The MBOSS color distributions will now be compared individually with a continuous distribution model, and with a bimodal distribution. The model distributions which are chosen are extremely simple; indeed, the idea is not to find a physical model that reproduces the data, but just to decide if the observed sample is compatible or not with a type of distribution. The model parameters are the following:

- Continuous distribution: the colors are uniformly distributed between C_1 and C_2;
- Bimodal distributions: the colors are uniformly distributed between B_1 and B_2 (group 1), and between B_3 and B_4 (if $B_1 = B_2$ and $B_3 = B_4$, the two "blobs" have no internal spread). An additional parameter f gives the fraction of TNOs in the first blob. We impose a requirement that $B_3 - B_2 > 0.2$ mag, i.e. that there is a clear separation between the two blobs of a bimodal distribution. We adjust the parameters to maximize $Prob$.

For each color index, we considered the 2 models for the Plutinos, the Cubewanos and both Plutinos and Cubewanos together. The parameters of the models, as well as the corresponding probabilities, are available in Table 5. Figure 6 displays examples of the CPF for the TNO color indexes and the corresponding models.

Results:

- Plutinos and Cubewanos have color distributions that are compatible with a simple, uniform, continuous distribution (the worse probability is ∼4% for the Cubewanos' and Plutinos+Cubewanos' $B-I$);
- Some of the color distributions are not compatible with a bimodal distribution as defined (i.e. no adjustment of the distribution parameter can give a probability of compatibility larger than a few percent). These are the Plutinos' $B-V$ and $V-R$, and the Cubewanos' $V-R$ and $R-I$. When considering both classes together, the $V-R$, $V-I$ and $R-I$ are not compatible with a bimodal distribution.

Table 6. Parameters of the models maximizing the KS statistics for the 2D distribution of TNO colors, and corresponding d and $Prob$. The table is available in electronic form at `http://www.edpsciences.org`.

6.2. 2D distributions

The traditional color indexes ($B-V, V-R, R-I$, etc., but also $B-I, B-K, R-J$, etc) are based on the standard photometric systems. There is no reason to believe that this system is specially adequate for TNO or Centaur work. It is possible that groups would appear in 2D (or >2D) diagrams, that would not appear in the 1D distributions. An illustration of this is the clustering of the MBOSSes around the reddening line, an effect that would not be visible in the 1D distributions. In this section, we will re-do a similar KS analysis in various 2-dimension space. Ideally, we could extend this work to a N-dimension space. Unfortunately, the KS tool does not exist for D > 2.

As in the 1D case, we will compare the observed distributions with model distributions. We will also use a bimodal model, in which the colors are spread around 2 individual points in the color-color diagram, and a continuous model, in which the colors are spread around a line joining 2 points in the color-color diagram. In order to simulate these model distributions, a large number (10 000) of test objects is created at random. The observed distribution is then compared to the model population. We verified that the resulting P are not significantly varying for larger model sample, nor for one random population to the next.

In addition to the coordinates of the center of both blobs in the color-color diagram being considered, the parameters of the models are the spread of the distribution in x and y and, in case of a bimodal distribution, the fraction of the population in the first blob. The parameters were adjusted iteratively in order to maximize the KS probability.

Table 6 lists the parameters of the models giving the higher P and the corresponding values of d and P. Examples of the random populations simulating the models have been plotted on the color-color diagrams displayed in Fig. 7.

Results: Adjusting the parameters of the model distributions, we could obtain fairly high values of $Prob$ in all cases except for the $B-V/R-I$ and $B-V/V-R$ diagrams for Plutinos and Cubewanos, that cannot be reproduced by a bimodal distribution. In other words, all the 2D distributions considered are compatible with both continuous *and*

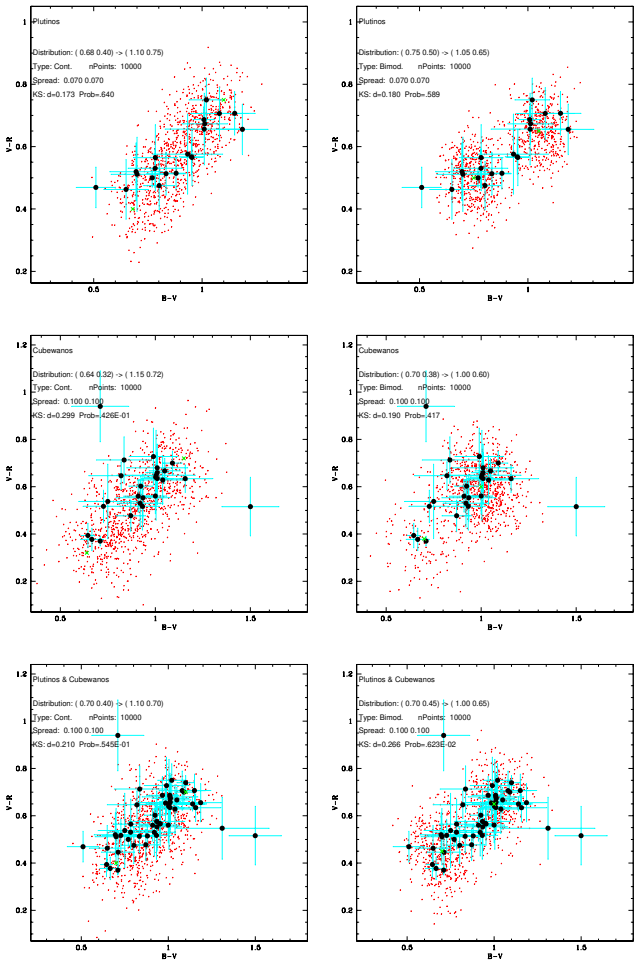

Fig. 7. Examples of color-color diagrams of the TNOs, superimposed to the model distributions used for the KS analysis described in the text. Left column corresponds to continuous distributions, right to bimodal. Top row is for Plutinos, middle for Cubewanos, bottom for both together.

bimodal distributions, except the 2 diagrams mentioned above, which are not compatible with (simple) bimodal distributions.

7. Discussion and summary

7.1. Dataset

We compiled the colors of Minor Bodies in the Outer Solar System from 40 references, totaling measurements during 486 epochs of 104 objects, i.e. 13 SP Comets, 14 Centaurs, 9 Scattered TNOs, 20 Plutinos and 48 Cubewanos. For each object, these measurements have been carefully combined, taking care not to introduce rotational artifacts in the colors, and weighting each measurement with its error bar. The final error bar reflects the combined signal/noise ratio and the dispersion between the measurements. The absolute R magnitudes ($M(1,1)$) and the mean reflectivity slope $\mathcal{S}$ have been computed for each object, together with the deviation from a linear spectrum. The color-color diagrams are presented. The mean of each color (and its error) is presented for all the MBOSS classes.

7.2. Individual objects

A small group of objects – 1995 SM_{55}, 1996 TL_{66}, 1999 OY_3, 1996 TO_{66} and (2060) Chiron – have almost perfectly solar colors, suggesting they are covered with neutrally colored fresh ice. Chiron is known to be cometary active, and 1996 TO_{66} is suspected to be so too. The other objects from this group therefore deserve a closer study to look for activity and/or fresh ice spectral signature.

Four objects appear as outliers from the general population: 1994 ES_2, 1994 EV_3, 1998 HK_{151} and 1995 DA_2. In all cases, we suspect that they do not correspond to physically distinct objects, but that the colors reported are not accurate.

7.3. Gradient and colors

In the color-color diagram, the objects follow closely the "reddening line" (which is the locus of objects having a linear reflectivity spectrum). This confirms that most MBOSSes have globally linear reflectivity spectra in the visible. Nevertheless, some systematic effects are visible:

- The diagrams involving the I band indicate that the spectrum of many objects becomes flatter toward the near-IR, which is expected if one considers the laboratory spectra.
- Also, many objects present a bend in the B region. The latter is not matching the laboratory spectra for fresh ices. Maybe they correspond to objects in an evolved state (e.g. covered with extremely irradiated ices, which can have reflectivity spectra bend in the blue region), as opposed to having recently been re-surfaced.

7.4. Correlations with orbital elements

7.4.1. Semi-major axis a

There is no correlation between the color (and spectral gradient) of the objects and their orbit semi-major axis. This stands for the whole MBOSS population as well as for the individual families. Therefore, the traditional increasing reddening of asteroids with a that is observed for Main-Belt asteroids and Trojans stands for the MBOSSes as a whole (i.e. they are on average considerably redder than objects closer to the Sun, cf. Table 4), but not within the MBOSSes themselves.

7.4.2. Orbit excitation i, e and $\mathcal{E}$

For the Plutinos, Centaurs and Scattered TNOS, the correlation between colors (including spectral gradient) and the other orbital parameters is either nonexistent or very weak: no trend is apparent in the different color vs. parameter plots, and this is confirmed by weak correlation coefficients and statistical tests.

One notable exception: the color of the Cubewanos presents a very strong, very significant correlation with the eccentricity, inclination and "excitation" ($\mathcal{E}$ obtained

by combining quadratically i and e): Cubewanos with a small excitation are systematically and significantly redder than those with a higher excitation. This confirms the results presented by Trujillo et al. (2001) and Stern (oral comm. at Meudon 2001 workshop), who obtained similar correlations on smaller samples.

In addition, the Cubewanos with large orbital excitation have significantly broader color distributions than the others.

In a more general way, the difference is greater between Cubewanos with a small and large orbital excitation than the difference between the different classes of MBOSSes.

This suggests either that

- objects with higher excitation suffer a more efficient resurfacing, because of more numerous and stronger collisions than those with smaller excitation, or that
- objects with low excitation constitute a different population, possibly covered with a more primordial surface, or of a different nature.

7.5. Absolute magnitude

The tests involving the absolute magnitude of the object ($M(1,1)$, neglecting the solar phase correction, which is unknown but expected to be small) deserve special attention.

Cubewanos with faint $M(1,1)$ tend to be redder than the others (this effect is visible through the correlation coefficients and the t-tests). Plutinos present the opposite trend (faint $M(1,1)$ tend to be bluer), with about the same significance. It is difficult to explain this through a selection effect at discovery. However, the Plutinos extend to fainter $M(1,1)$ than the Cubewanos (a effect of the latter being on average further away from the Sun, therefore fainter than Plutinos of the same absolute magnitude). At this point, these opposite trends are not explained.

The width of the color distributions of the objects with faint $M(1,1)$ is never significantly different than those of the larger objects. The models of collisional resurfacing balancing the reddening (Luu & Jewitt 1996a; Jewitt & Luu 2001) predict that the smaller objects will have a broader range of colors, which is not observed. Therefore, the current database does not support this model. Jewitt & Luu (2001) discuss also that, for that model, the colors of a given object should vary with same amplitude as the variation of colors between objects of the same diameters, which is not the case. However, as this database does not explore the rotational variations, this cannot be further explored.

7.6. Comparison between populations

The color distribution of the Scattered TNOs systematically cover a narrower range than those of the other classes; this is not substantiated by the statistical tests, but possibly because the distributions have fairly different shapes. Nevertheless, if confirmed in the future, this would indicate that they are on average exposed to a narrower range of resurfacing effects – for instance, less collisions because they spend a significant fraction of their time far out of the densely populated regions, or strictly no cometary activity because they are the most distant objects from the Sun. This could give constraints on the conditions to which they are exposed.

We performed a series of statistical tests on the color distributions (f-test, t-test and KS). These tests indicate that the comets' colors are significantly bluer than those of the other MBOSSes. This result is very strong for the Cubewanos and Plutinos (with a probability that the comet are actually similar to these objects of $\sim 10^{-3}$ on individual color indexes), and weaker for the Centaurs and Scattered TNOs (probability of the order of a %).

There is no evidence that the Plutinos, Cubewanos, Centaurs and Scattered TNOs have significantly different color distributions.

Non-physical, arbitrary populations (in which the objects are distributed according to their designation) were used to test the statistical methods; they indicate that probabilities larger than ∼5–10% should not be considered as reliable.

7.7. Bimodality of the color distributions

Visually comparing the color CPFs of the various classes, it appears that the Cubewanos and Centaurs tend to have "bimodal" (2 well separated steps) or "broken" (2 well separated slopes) distributions, while the Plutinos tend to have very continuous distributions (i.e. uniform CPF slope over the whole range).

However, statistical comparison of the observations with simple 1D and 2D model distributions indicate that, in no case we have enough data to rule out the validity of simple, continuous distributions to represent the data. This does not mean that the distributions are continuous, but that we have to be extremely careful if saying that they are not.

Jewitt & Luu (2001) have performed some statistical tests (bin, dip and interval distribution tests) on a smaller sample; these tests do not provide evidence that the $B-V$ and $V-R$ of their sample are distributed bimodally.

7.8. Prospects

We plan to maintain and update the observations database and keep it available on the web (at `http://www.sc.eso.org/~ohainaut/MBOSS`). We encourage the observers to send us the tables of their publications electronically. We intend to update this paper when the number objects in the database will have doubled or when the conclusions will have significantly changed.

Appendix A: Color measurement references

The list of papers that were used for each object to build this database is available in the electronic form at

http://www.edpsciences.org, and maintained on our web site http://www.sc.eso.org/~ohainaut/MBOSS

Appendix B: Statistical tests

In this appendix, we describe in detail the statistical tests used thorough this paper.

B.1. Correlation coefficient

Pearson's correlation coefficient r evaluates the association between two continuous variables x and y (such as the orbit semi-major axis a and the $V-R$ color). r is given by

$$r = \frac{\sum_i (x_i - \bar{x})(y_i - \bar{y})}{\sqrt{\sum_i (x_i - \bar{x})^2} \sqrt{\sum_i (y_i - \bar{y})^2}} \quad \text{(B.1)}$$

where $\bar{x}$ and $\bar{y}$ are the mean of x and y. r is in the $-1, 1$ range. Large values (positive or negative) indicate a strong correlation between the two variables, while a value close to 0 indicates that they are uncorrelated. Unfortunately, there is no reliable way to quantify the significance of that correlation for small samples (less than 500 elements).

B.2. Comparing two distributions

The tests described in this section aim at comparing two continuous, 1D distributions (such as the $V-R$ colors of two MBOSS families). These three tests estimate the validity of the null hypothesis "the two samples are extracted from the same population." This is performed by computing an estimator (f, t and d resp., defined below), whose direct interest is limited. From the estimator, a much more interesting value is derived: *Prob*, the probability that the statistical estimator is as large as measured *by chance*. *Prob* is the probability to get a statistical estimator as large as or larger than the value measured while the two samples compared being actually random sub-samples of a same distribution. Large values of *Prob* indicate that it is very probable to get the measured estimator by chance, or in other words, that we have no reason to claim (on statistical bases) that the two samples come from different distributions. Remember, however, that this does not allow us to say that the samples are identical, only that they are not statistically incompatible. On the other hand, small values of *Prob* indicate that the chances of getting the observed estimator by chance while extracting the two samples from the same distributions are small, or in other words, that the two samples are not statistically compatible. The size of the sub-samples is taken into account in the computation of *Prob*. While it is definitely safer to work on "large" samples, the advantage of these methods is that they start to give fairly reliable results with fairly small samples; in this study, we set the threshold as ≥ 7. The probability at which one can conclude that samples are different depends on the certainty level required. Traditional values are 0.05 and 0.003, corresponding to the usual 2 and 3σ levels. For this study, we will start raising the warning flags at $Prob \leq 0.1$. Of course, if we raise 10 such flags, we can expect that one of them will be a random effect.

The statistic tests are described in more detail, together with their original references and with the algorithms we used in Press et al. (1992).

B.2.1. Student's t test

This test checks whether the means of two distributions are significantly different. The basic implementation of this test implies that the variance of both distributions are equal. For the MBOSSes colors, this cannot be guaranteed (we deal with that question with the next section). We therefore used a modified version of the t test that deals with unequal variances:

$$t = \frac{\overline{x_A} - \overline{x_B}}{(\mathrm{Var}(x_A)/N_A + \mathrm{Var}(x_B)/N_B)^{1/2}}, \quad \text{(B.2)}$$

where x_A and x_B are the two color distributions considered, $\overline{x}$ and $\mathrm{Var}(x)$ their means and variances, and N the number of objects. The statistic *Prob* of t is distributed approximately as the original Student's t, and is given by the Student's distribution probability function A, which is related to the incomplete beta function (see Press et al. 1992, for details). Small values of *Prob* indicate that the distributions are different.

B.2.2. f test

The f-test evaluates whether two distributions have significantly different variances. The statistic f is simply the ratio of the largest variance to the smaller one:

$$f = \frac{\mathrm{Var}(x_A)}{\mathrm{Var}(x_B)}. \quad \text{(B.3)}$$

Very large values of f indicate that the difference is significant. *Prob*, the statistics of F, is obtained by the f-distribution probability function, which is related to the incomplete beta function.

B.2.3. Kollmogorov-Smirnov test

Obviously, the whole information from a distribution is not contained in its two first moments (mean and variance). A more complete comparison of the color distributions is therefore interesting. The ideal statistics tool for this purpose is the Kolmogorov-Smirnov (KS) test. The distributions are compared through their Cumulative Probability Function (CPF) $S(x)$, which is defined as the fraction of the sample whose value is smaller or equal to x. f starts at 0 and increases till it reaches 1 for the x corresponding to largest element of the distribution. d, the KS test, is the maximum (vertical) distance between the CPFs S_1 and S_2 of the samples to be compared, i.e.

$$d = \max_{-\infty < x < \infty} |S_1(x) - S_2(x)|. \quad \text{(B.4)}$$

The distribution of d's statistic can be calculated: the probability to get a d larger than the observed one, the

Table C.1. Size, mean and square-root of the variance of the sub-samples used for statistical tests (for a description of the sub-samples, see Sect. 3), whose results are listed in the right-most columns. The correlation coefficient (last column) is computed on the whole sample. This table refers to the whole MBOSS population (left) and the Cubewanos only (right).

All MBOSS populations

Col.	Pop. 1 (small)		Pop. 2 (large)		Statistics		
	n_1	$\bar{x}/\sigma$	n_2	$\bar{x} \pm \sigma$	$t/Prob$	$f/Prob$	r
vs. a: semi-major axis. $a_{\rm cut} = 42.00$AU							
$B-V$	39	0.91/0.20	36	0.93/0.17	−0.40/0.691	1.33/0.396	−0.01
$B-R$	39	1.49/0.29	33	1.53/0.26	−0.72/0.476	1.30/0.451	0.00
$B-I$	34	2.04/0.44	29	2.08/0.35	−0.40/0.690	1.62/0.194	−0.06
$V-R$	42	0.59/0.12	40	0.61/0.14	−0.67/0.508	1.40/0.292	0.02
$V-I$	34	1.14/0.25	33	1.18/0.24	−0.70/0.486	1.03/0.932	−0.02
$V-J$	11	2.05/0.49	5	1.62/0.41	1.77/0.109	1.43/0.783	−0.05
$R-I$	35	0.56/0.14	33	0.60/0.14	−1.29/0.200	1.02/0.941	0.00
$I-J$	6	0.69/0.23	0	—	—/—	—/—	—
$J-H$	8	0.43/0.32	4	0.27/0.36	—/—	—/—	—
$H-K$	7	0.02/0.07	3	0.22/0.51	—/—	—/—	—
$\mathcal{S}$	40	22.86/13.09	37	25.44/14.58	−0.81/0.418	1.24/0.510	0.01
vs. e: eccentricity. $e_{\rm cut} = 0.18$							
$B-V$	34	0.94/0.19	42	0.90/0.18	0.99/0.324	1.10/0.772	−0.08
$B-R$	32	1.54/0.26	41	1.48/0.29	0.93/0.358	1.30/0.450	−0.09
$B-I$	25	2.14/0.34	38	2.01/0.43	1.26/0.214	1.55/0.258	−0.04
$V-R$	40	0.61/0.13	44	0.59/0.12	0.75/0.455	1.14/0.678	−0.12
$V-I$	29	1.19/0.23	40	1.12/0.25	1.25/0.216	1.14/0.718	−0.12
$V-J$	6	1.81/0.47	11	1.96/0.50	−0.63/0.543	1.12/0.954	0.01
$R-I$	28	0.60/0.14	42	0.56/0.15	1.35/0.183	1.08/0.851	−0.15
$I-J$	1	0.73/—	6	0.69/0.24	—/—	—/—	—
$J-H$	4	0.29/0.36	9	0.42/0.30	—/—	—/—	—
$H-K$	3	0.27/0.48	8	0.00/0.06	—/—	—/—	—
$\mathcal{S}$	36	24.73/14.03	42	22.71/13.60	0.64/0.522	1.06/0.843	−0.07
vs. i: inclination. $i_{\rm cut} = 6.94^\circ$							
$B-V$	38	0.93/0.20	38	0.91/0.17	0.51/0.614	1.50/0.225	−0.17
$B-R$	36	1.53/0.27	37	1.48/0.29	0.65/0.517	1.11/0.760	−0.22
$B-I$	32	2.09/0.38	31	2.03/0.42	0.57/0.568	1.20/0.618	−0.18
$V-R$	43	0.62/0.12	42	0.58/0.13	1.29/0.201	1.08/0.800	−0.28
$V-I$	36	1.18/0.23	34	1.12/0.25	1.11/0.270	1.22/0.570	−0.22
$V-J$	6	1.89/0.52	11	1.91/0.49	−0.09/0.932	1.11/0.830	−0.18
$R-I$	36	0.59/0.14	35	0.56/0.14	1.04/0.303	1.01/0.982	−0.15
$I-J$	2	0.43/0.06	5	0.80/0.14	—/—	—/—	—
$J-H$	5	0.47/0.42	8	0.32/0.24	0.73/0.497	2.96/0.200	−0.38
$H-K$	4	−0.01/0.07	7	0.12/0.31	—/—	—/—	—
$\mathcal{S}$	39	26.02/13.31	40	21.67/13.98	1.42/0.161	1.10/0.766	−0.22
vs. $\mathcal{E} = \sqrt{e^2+i^2}$: orbit excitation. $\mathcal{E}_{\rm cut} = 0.28$							
$B-V$	36	0.93/0.19	40	0.90/0.18	0.72/0.473	1.18/0.606	−0.17
$B-R$	34	1.54/0.24	39	1.47/0.30	1.17/0.246	1.53/0.214	−0.21
$B-I$	29	2.10/0.34	34	2.03/0.44	0.74/0.462	1.66/0.177	−0.15
$V-R$	41	0.62/0.11	43	0.57/0.13	1.98 /**0.051**	1.29/0.423	−0.25
$V-I$	33	1.20/0.21	36	1.11/0.26	1.52/0.133	1.48/0.265	−0.21
$V-J$	5	1.88/0.41	12	1.92/0.53	−0.14/0.889	1.63/0.676	−0.10
$R-I$	32	0.60/0.14	38	0.56/0.15	1.16/0.251	1.08/0.834	−0.20
$I-J$	1	0.39/—	6	0.75/0.18	—/—	—/—	—
$J-H$	4	0.64/0.40	9	0.27/0.19	—/—	—/—	—
$H-K$	2	−0.07/0.04	9	0.11/0.27	—/—	—/—	—
$\mathcal{S}$	38	25.88/13.01	40	21.52/14.25	1.41/0.162	1.20/0.580	−0.19
vs. $M(1,1)$: absolute magnitude. $M(1,1)_{\rm cut} = 6.86$							
$B-V$	34	0.92/0.14	34	0.93/0.23	−0.09/0.928	2.45 /**0.012**	0.02
$B-R$	32	1.51/0.26	34	1.51/0.30	0.01/0.991	1.28/0.498	−0.01
$B-I$	31	2.08/0.36	26	2.06/0.44	0.21/0.835	1.53/0.267	0.03
$V-R$	40	0.61/0.13	37	0.60/0.12	0.33/0.745	1.22/0.550	0.00
$V-I$	34	1.17/0.22	29	1.15/0.26	0.41/0.687	1.38/0.375	−0.01
$V-J$	8	1.69/0.46	6	2.25/0.35	−2.60 /**0.023**	1.72/0.569	0.45
$R-I$	33	0.58/0.12	30	0.56/0.16	0.53/0.599	1.88 /**0.085**	−0.01
$I-J$	2	0.60/0.18	2	0.87/0.25	—/—	—/—	—
$J-H$	7	0.31/0.26	4	0.52/0.46	—/—	—/—	—
$H-K$	6	0.13/0.34	3	0.03/0.07	—/—	—/—	—
$\mathcal{S}$	36	24.13/12.37	36	23.97/15.15	0.05/0.960	1.50/0.235	−0.01

Cubewanos population

Col.	Pop. 1 (small)		Pop. 2 (large)		Statistics		
	n_1	$\bar{x} \pm \sigma$	n_2	$\bar{x} \pm \sigma$	$t/Prob$	$f/Prob$	r
vs. a: semi-major axis. $a_{\rm cut} = 43.80$AU							
$B-V$	13	0.97/0.23	14	0.89/0.12	1.14/0.270	3.78 /**0.024**	−0.29
$B-R$	13	1.52/0.31	11	1.57/0.14	−0.48/0.639	5.23 /**0.013**	0.02
$B-I$	8	2.04/0.43	12	2.16/0.20	−0.75/0.471	4.50 /**0.027**	0.11
$V-R$	17	0.59/0.13	16	0.67/0.13	−1.66/0.108	1.00/1.000	0.07
$V-I$	9	1.09/0.24	15	1.27/0.20	−1.86 /**0.083**	1.47/0.504	0.30
$V-J$	1	1.00 ± —	3	1.89/0.16	—/—	—/—	—
$R-I$	9	0.59/0.18	15	0.63/0.12	−0.71/0.494	2.43/0.140	0.17
$I-J$	0	—	0	—	—/—	—/—	—
$J-H$	1	−0.21 ± —	2	0.47/0.25	—/—	—/—	—
$H-K$	1	0.81 ± —	1	−0.10 ± —	—/—	—/—	—
$\mathcal{S}$	13	21.27 ± 12.29	15	29.95 ± 15.63	−1.64/0.112	1.62/0.410	0.17
vs. e: eccentricity. $e_{\rm cut} = 0.07$							
$B-V$	12	1.05/0.16	15	0.83/0.12	5.72 /**0.000**	1.76/0.274	−0.58
$B-R$	12	1.67/0.16	12	1.41/0.25	3.94 /**0.001**	5.01 /**0.003**	−0.57
$B-I$	8	2.27/0.11	12	2.00/0.36	3.75 /**0.002**	8.19 /**0.001**	−0.45
$V-R$	17	0.65/0.11	16	0.60/0.16	1.38/0.178	2.69 /**0.039**	−0.19
$V-I$	10	1.23/0.11	14	1.18/0.28	1.66/0.112	7.32 /**0.001**	−0.15
$V-J$	1	2.07 ± —	3	1.53/0.46	—/—	—/—	—
$R-I$	10	0.64/0.12	14	0.60/0.16	1.38/0.180	2.62 /**0.079**	0.01
$I-J$	0	—	0	—	—/—	—/—	—
$J-H$	1	0.30 ± —	2	0.22/0.61	—/—	—/—	—
$H-K$	1	−0.10 ± —	1	0.81 ± —	—/—	—/—	—
$\mathcal{S}$	13	28.05/6.59	15	24.08 ± 19.13	0.75/0.461	8.43 /**0.001**	−0.26
vs. i: inclination. $i_{\rm cut} = 3.75^\circ$							
$B-V$	14	1.01/0.18	13	0.84/0.13	2.41 /**0.023**	1.72/0.283	−0.51
$B-R$	13	1.68/0.14	11	1.38/0.24	3.86 /**0.001**	7.09 /**0.000**	**−0.76**
$B-I$	10	2.30/0.14	10	1.92/0.32	4.15 /**0.001**	7.30 /**0.001**	**−0.71**
$V-R$	19	0.69/0.11	14	0.54/0.12	3.12 /**0.004**	2.46 /**0.052**	−0.58
$V-I$	14	1.30/0.19	10	1.06/0.20	4.15 /**0.000**	1.89/0.214	−0.59
$V-J$	1	2.07 ± —	3	1.53/0.46	—/—	—/—	—
$R-I$	14	0.66/0.13	10	0.55/0.14	3.00 /**0.006**	1.39/0.516	−0.41
$I-J$	0	—	0	—	—/—	—/—	—
$J-H$	1	0.30 ± —	2	0.22/0.61	—/—	—/—	—
$H-K$	1	−0.10 ± —	1	0.81 ± —	—/—	—/—	—
$\mathcal{S}$	16	33.31 ± 13.38	12	16.07/9.69	3.95 /**0.001**	1.91/0.284	**−0.61**
vs. $\mathcal{E} = \sqrt{e^2+i^2}$: orbit excitation. $\mathcal{E}_{\rm cut} = 0.13$							
$B-V$	14	1.01/0.18	13	0.84/0.13	2.95 /**0.006**	1.13/0.808	−0.59
$B-R$	13	1.68/0.14	11	1.38/0.24	4.24 /**0.000**	6.16 /**0.001**	**−0.77**
$B-I$	10	2.30/0.14	10	1.92/0.32	4.55 /**0.000**	6.62 /**0.002**	**−0.72**
$V-R$	19	0.69/0.11	14	0.54/0.12	3.63 /**0.001**	1.64/0.289	−0.55
$V-I$	14	1.30/0.19	10	1.06/0.20	3.99 /**0.000**	1.80/0.260	−0.54
$V-J$	1	2.07 ± —	3	1.53/0.46	—/—	—/—	—
$R-I$	14	0.66/0.13	10	0.55/0.14	3.13 /**0.004**	1.24/0.671	−0.36
$I-J$	0	—	0	—	—/—	—/—	—
$J-H$	1	0.30 ± —	2	0.22/0.61	—/—	—/—	—
$H-K$	1	−0.10 ± —	1	0.81 ± —	—/—	—/—	—
$\mathcal{S}$	16	33.31 ± 13.38	12	16.07/9.69	3.95 /**0.001**	1.91/0.284	−0.58
vs. $M(1,1)$: absolute magnitude. $M(1,1)_{\rm cut} = 6.73$							
$B-V$	14	0.90/0.16	9	0.97/0.23	−0.84/0.414	1.96/0.270	0.31
$B-R$	12	1.47/0.28	9	1.64/0.19	−1.61/0.125	2.18/0.277	0.53
$B-I$	11	2.01/0.36	7	2.23/0.21	−1.62/0.125	2.86/0.211	**0.66**
$V-R$	18	0.59/0.14	12	0.69/0.13	−2.02 /**0.054**	1.22/0.758	0.53
$V-I$	13	1.12/0.20	9	1.30/0.24	−1.85 /**0.084**	1.41/0.570	**0.62**
$V-J$	4	1.67/0.47	0	—	—/—	—/—	—
$R-I$	12	0.55/0.12	9	0.67/0.15	−1.94 /**0.072**	1.70/0.408	**0.62**
$I-J$	0	—	0	—	—/—	—/—	—
$J-H$	3	0.25/0.43	0	—	—/—	—/—	—
$H-K$	2	0.35/0.64	0	—	—/—	—/—	—
$\mathcal{S}$	15	20.30 ± 11.41	10	34.10 ± 17.43	−2.21 /**0.044**	2.33/0.150	0.53

two data sets being drawn from the same distribution, is given by

$$Prob(d > \text{observed}) = Q_{\rm KS}\left((\sqrt{N_{\rm e}} + 0.12 + 0.11/\sqrt{N_{\rm e}})\, d\right), \quad \text{(B.5)}$$

where $N_{\rm e}$ is the effective number of data points,

$$N_{\rm e} = \frac{N_1 N_2}{N_1 + N_2}, \quad \text{(B.6)}$$

and the function $Q_{\rm KS}$ is defined as

$$Q_{\rm KS}(\lambda) = 2\sum_{j=1}^{\inf}(-1)^{j-1} e^{-2j^2\lambda^2}. \quad \text{(B.7)}$$

Appendix C: Results of the statistical tests

This appendix presents the detailed results of the statistical tests described in the paper. Tables C.3, C.5 and C.6 concern the comparison between the colors of the various classes of MBOSSes.

Table C.1. Continued, for Plutinos only (left) and Centaurs/Scattered TNOs only (right).

Plutinos population

Col.	Pop. 1 (small)		Pop. 2 (large)		Statistics		
	n_1	$\bar{x} \pm \sigma$	n_2	$\bar{x} \pm \sigma$	$t/Prob$	$f/Prob$	r
vs. a: semi-major axis. $a_{\rm cut} = 38.70$AU							
$B-V$	14	0.87/0.17	6	0.92/0.20	−0.59/0.572	1.31/0.636	0.16
$B-R$	14	1.44/0.25	6	1.52/0.31	−0.58/0.578	1.53/0.493	0.20
$B-I$	11	1.93/0.37	6	2.07/0.51	−0.59/0.573	1.88/0.370	0.10
$V-R$	14	0.57/0.10	6	0.61/0.08	−0.97/0.351	1.42/0.740	0.21
$V-I$	11	1.08/0.20	6	1.19/0.31	−0.79/0.452	2.45/0.214	0.15
$V-J$	0	—	4	2.35/0.21	—/—	—/—	—
$R-I$	11	0.52/0.14	6	0.58/0.20	−0.70/0.507	2.18/0.276	0.10
$I-J$	0	—	0	—	—/—	—/—	—
$J-H$	1	1.20 ± —	1	0.40 ± —	—/—	—/—	—
$H-K$	0	—	1	−0.04 ± —	—/—	—/—	—
$\mathcal{S}$	14	20.32 ± 11.91	6	25.13 ± 13.68	−0.75/0.475	1.32/0.631	0.19
vs. e: eccentricity. $e_{\rm cut} = 0.23$							
$B-V$	10	0.92/0.20	10	0.85/0.15	0.99/0.337	1.83/0.382	−0.19
$B-R$	10	1.51/0.30	10	1.42/0.23	0.71/0.486	1.70/0.443	−0.14
$B-I$	8	2.09/0.48	9	1.88/0.33	1.05/0.312	2.10/0.319	−0.34
$V-R$	10	0.60/0.09	10	0.56/0.10	0.99/0.336	1.22/0.774	−0.09
$V-I$	8	1.17/0.27	9	1.07/0.21	0.83/0.422	1.67/0.485	−0.25
$V-J$	2	2.43/0.00	2	2.26/0.32	—/—	—/—	—
$R-I$	8	0.57/0.18	9	0.52/0.15	0.70/0.498	1.49/0.587	−0.21
$I-J$	0	—	0	—	—/—	—/—	—
$J-H$	1	0.40 ± —	1	1.20 ± —	—/—	—/—	—
$H-K$	1	−0.04 ± —	0	—	—/—	—/—	—
$\mathcal{S}$	10	23.66 ± 11.96	10	19.86 ± 12.98	0.68/0.504	1.18/0.812	−0.09
vs. i: inclination. $i_{\rm cut} = 5.30^\circ$							
$B-V$	10	0.88/0.16	10	0.90/0.20	−0.25/0.808	1.54/0.532	0.24
$B-R$	10	1.43/0.23	10	1.50/0.29	−0.55/0.591	1.57/0.515	0.32
$B-I$	9	1.98/0.35	8	1.98/0.50	0.00/0.996	2.03/0.342	0.24
$V-R$	10	0.57/0.09	10	0.59/0.10	−0.65/0.521	1.30/0.701	0.26
$V-I$	9	1.14/0.21	8	1.09/0.28	0.38/0.711	1.84/0.411	0.15
$V-J$	2	2.23/0.29	2	2.46/0.03	—/—	—/—	—
$R-I$	9	0.57/0.14	8	0.51/0.19	0.66/0.521	1.83/0.415	0.09
$I-J$	0	—	0	—	—/—	—/—	—
$J-H$	2	0.80/0.57	0	—	—/—	—/—	—
$H-K$	1	−0.04 ± —	0	—	—/—	—/—	—
$\mathcal{S}$	10	20.80 ± 10.97	10	22.72 ± 14.05	−0.34/0.739	1.64/0.473	0.26
vs. $\mathcal{E} = \sqrt{e^2 + i^2}$: orbit excitation. $\mathcal{E}_{\rm cut} = 0.27$							
$B-V$	10	0.88/0.20	10	0.89/0.16	−0.19/0.849	1.42/0.606	0.03
$B-R$	10	1.45/0.28	10	1.48/0.25	−0.29/0.772	1.28/0.721	0.10
$B-I$	9	1.98/0.43	8	1.97/0.42	0.07/0.942	1.04/0.976	−0.08
$V-R$	10	0.59/0.09	10	0.57/0.09	0.29/0.773	1.09/0.902	0.06
$V-I$	9	1.12/0.25	8	1.12/0.25	0.04/0.965	1.02/0.992	−0.08
$V-J$	1	2.43 ± —	3	2.32/0.25	—/—	—/—	—
$R-I$	9	0.54/0.17	8	0.54/0.16	−0.05/0.962	1.16/0.858	−0.08
$I-J$	0	—	0	—	—/—	—/—	—
$J-H$	2	0.80/0.57	0	—	—/—	—/—	—
$H-K$	1	−0.04 ± —	0	—	—/—	—/—	—
$\mathcal{S}$	10	21.60 ± 12.11	10	21.92 ± 13.15	−0.06/0.955	1.18/0.811	0.08
vs. $M(1,1)$: absolute magnitude. $M(1,1)_{\rm cut} = 7.42$							
$B-V$	10	0.93/0.21	10	0.85/0.14	1.01/0.330	2.36/0.217	−0.29
$B-R$	10	1.53/0.29	10	1.40/0.22	1.19/0.252	1.64/0.471	−0.30
$B-I$	9	2.14/0.43	8	1.79/0.32	1.94 /**0.073**	1.81/0.450	−0.44
$V-R$	10	0.60/0.09	10	0.56/0.09	0.93/0.364	1.20/0.792	−0.27
$V-I$	9	1.21/0.22	8	1.01/0.23	1.82 /**0.089**	1.03/0.956	−0.41
$V-J$	2	2.43/0.00	2	2.26/0.32	—/—	—/—	—
$R-I$	9	0.60/0.15	8	0.47/0.15	1.83 /**0.088**	1.04/0.944	−0.42
$I-J$	0	—	0	—	—/—	—/—	—
$J-H$	1	0.40 ± —	1	1.20 ± —	—/—	—/—	—
$H-K$	1	−0.04 ± —	0	—	—/—	—/—	—
$\mathcal{S}$	10	24.84 ± 11.54	10	18.68 ± 12.86	1.13/0.275	1.24/0.752	−0.30

Centaur and Scattered TNO populations

Col.	Pop. 1 (small)		Pop. 2 (large)		Statistics		
	n_1	$\bar{x} \pm \sigma$	n_2	$\bar{x} \pm \sigma$	$t/Prob$	$f/Prob$	r
vs. a: semi-major axis. $a_{\rm cut} = 24.40$AU							
$B-V$	11	0.91/0.23	11	0.91/0.17	0.00/1.000	1.86/0.343	−0.06
$B-R$	11	1.48/0.36	11	1.47/0.30	0.03/0.978	1.46/0.564	−0.11
$B-I$	10	2.10/0.52	11	2.00/0.43	0.46/0.648	1.46/0.560	−0.16
$V-R$	11	0.58/0.15	11	0.56/0.13	0.23/0.817	1.31/0.677	−0.15
$V-I$	10	1.17/0.29	10	1.08/0.25	0.70/0.492	1.34/0.672	−0.18
$V-J$	5	1.90/0.56	2	1.38/0.10	—/—	—/—	—
$R-I$	10	0.60/0.15	11	0.54/0.12	0.99/0.337	1.49/0.544	−0.16
$I-J$	5	0.74/0.20	1	0.39 ± —	—/—	—/—	—
$J-H$	5	0.34/0.05	1	0.35 ± —	—/—	—/—	—
$H-K$	5	0.03/0.08	1	−0.04 ± —	—/—	—/—	—
$\mathcal{S}$	11	24.00 ± 16.93	11	20.72 ± 12.36	0.52/0.610	1.87/0.336	−0.13
vs. e: eccentricity. $e_{\rm cut} = 0.38$							
$B-V$	12	0.87/0.20	11	0.95/0.18	−1.09/0.287	1.23/0.756	0.11
$B-R$	12	1.40/0.32	11	1.53/0.33	−0.97/0.344	1.07/0.902	0.07
$B-I$	11	1.96/0.47	10	2.15/0.46	−0.89/0.383	1.02/0.983	0.16
$V-R$	12	0.54/0.13	12	0.60/0.13	−1.10/0.282	1.05/0.935	0.10
$V-I$	11	1.09/0.25	11	1.14/0.28	−0.46/0.647	1.27/0.709	0.00
$V-J$	3	1.42/0.29	4	2.00/0.54	—/—	—/—	—
$R-I$	11	0.55/0.13	12	0.55/0.15	0.01/0.994	1.41/0.593	−0.07
$I-J$	3	0.53/0.18	3	0.84/0.18	—/—	—/—	—
$J-H$	2	0.35/0.09	4	0.34/0.03	—/—	—/—	—
$H-K$	2	0.08/0.02	4	−0.02/0.08	—/—	—/—	—
$\mathcal{S}$	12	19.15 ± 13.55	12	23.96 ± 14.97	−0.83/0.418	1.22/0.747	0.07
vs. i: inclination. $i_{\rm cut} = 13.20^\circ$							
$B-V$	12	0.91/0.19	11	0.90/0.21	0.20/0.845	1.24/0.729	−0.08
$B-R$	12	1.49/0.29	11	1.44/0.37	0.31/0.760	1.60/0.449	−0.13
$B-I$	10	2.11/0.45	11	2.00/0.49	0.56/0.583	1.21/0.785	−0.18
$V-R$	12	0.58/0.11	12	0.56/0.15	0.36/0.722	1.92/0.293	−0.16
$V-I$	10	1.13/0.25	12	1.10/0.28	0.27/0.790	1.27/0.736	−0.13
$V-J$	2	1.25/0.08	5	1.95/0.48	—/—	—/—	—
$R-I$	11	0.55/0.15	12	0.55/0.13	0.02/0.984	1.20/0.768	−0.06
$I-J$	2	0.43/0.06	4	0.81/0.16	—/—	—/—	—
$J-H$	1	0.29 ± —	5	0.35/0.04	—/—	—/—	—
$H-K$	1	0.06 ± —	5	0.00/0.08	—/—	—/—	—
$\mathcal{S}$	12	21.93 ± 12.32	12	21.18 ± 16.39	0.13/0.901	1.77/0.358	−0.09
vs. $\mathcal{E} = \sqrt{e^2 + i^2}$: orbit excitation. $\mathcal{E}_{\rm cut} = 0.44$							
$B-V$	12	0.88/0.19	11	0.94/0.19	−0.72/0.479	1.02/0.967	0.03
$B-R$	12	1.42/0.30	11	1.52/0.35	−0.71/0.488	1.38/0.601	−0.01
$B-I$	11	2.01/0.45	10	2.09/0.51	−0.40/0.692	1.29/0.694	0.02
$V-R$	12	0.55/0.12	12	0.59/0.14	−0.80/0.434	1.40/0.585	0.00
$V-I$	11	1.12/0.24	11	1.10/0.30	0.14/0.891	1.55/0.504	−0.08
$V-J$	3	1.42/0.29	4	2.00/0.54	—/—	—/—	—
$R-I$	11	0.58/0.12	12	0.53/0.15	0.83/0.416	1.49/0.539	−0.11
$I-J$	3	0.53/0.18	3	0.84/0.18	—/—	—/—	—
$J-H$	2	0.35/0.09	4	0.34/0.03	—/—	—/—	—
$H-K$	2	0.08/0.02	4	−0.02/0.08	—/—	—/—	—
$\mathcal{S}$	12	20.44 ± 12.69	12	22.67 ± 16.03	−0.38/0.710	1.60/0.450	0.00
vs. $M(1,1)$: absolute magnitude. $M(1,1)_{\rm cut} = 7.03$							
$B-V$	9	0.91/0.15	10	0.94/0.23	−0.36/0.726	2.30/0.256	−0.03
$B-R$	9	1.46/0.30	10	1.51/0.35	−0.38/0.706	1.37/0.671	−0.06
$B-I$	9	2.02/0.43	8	2.20/0.49	−0.81/0.432	1.30/0.719	0.06
$V-R$	10	0.56/0.13	10	0.59/0.12	−0.58/0.569	1.20/0.790	−0.08
$V-I$	10	1.10/0.26	8	1.17/0.25	−0.53/0.604	1.08/0.939	−0.02
$V-J$	3	1.46/0.27	2	2.13/0.68	—/—	—/—	—
$R-I$	10	0.55/0.14	9	0.58/0.14	−0.45/0.658	1.01/0.999	0.02
$I-J$	2	0.60/0.18	2	0.87/0.25	—/—	—/—	—
$J-H$	3	0.35/0.06	2	0.35/0.04	—/—	—/—	—
$H-K$	3	0.04/0.07	2	0.03/0.09	—/—	—/—	—
$\mathcal{S}$	10	20.87 ± 13.41	10	23.93 ± 14.06	−0.50/0.624	1.10/0.890	−0.09

Acknowledgements. We are very grateful to the authors of papers containing large tables who send us their measurements electronically, and to M. Vair, who compiled a significant fraction of the first versions of the database from the original papers. We also want to thank John Davies for accepting to undertake the task of reviewing this paper and for his numerous valuable comments. This research has made use of NASA's Astrophysics Data System Bibliographic Service.

Table C.2. f test: broadening of color and gradient distributions as a function of the absolute magnitude $M(1,1)$.

All MBOSS population									
Color	Cut	Blue Pop.			Red Pop.			Statistics	
		n_1	$\bar{x}$	σ	n_2	$\bar{x}$	σ	f	$prob$
$B-V$	0.94	34	7.00	1.55	34	6.73	1.57	1.02	0.947
$B-R$	1.56	33	7.03	1.74	33	6.77	1.38	1.58	0.202
$B-I$	2.13	28	6.73	1.58	29	6.77	1.60	1.02	0.957
$V-R$	0.60	38	6.92	1.53	39	6.79	1.42	1.17	0.639
$V-I$	1.18	31	6.80	1.54	32	6.72	1.55	1.01	0.984
$V-J$	1.82	7	6.02	1.53	7	6.86	0.84	3.34	0.168
$R-I$	0.58	31	6.91	1.48	32	6.64	1.59	1.15	0.706
$I-J$	0.69	2	0.00	0.00	2	0.00	0.00	14.61	0.326
$J-H$	0.32	5	6.39	1.74	6	6.57	0.92	3.58	0.195
$H-K$	−0.04	4	6.04	1.05	5	6.67	1.58	2.26	0.529
S	23.45	36	6.93	1.57	36	6.79	1.47	1.13	0.718
Plutinos population only									
Color	Cut	Blue Pop.			Red Pop.			Statistics	
		n_1	$\bar{x}$	σ	n_2	$\bar{x}$	σ	f	$prob$
$B-V$	0.88	10	7.66	0.43	10	6.73	1.22	7.94	0.005
$B-R$	1.40	10	7.66	0.43	10	6.73	1.22	7.94	0.005
$B-I$	1.78	8	7.70	0.43	9	6.58	1.19	7.56	0.015
$V-R$	0.56	10	7.66	0.43	10	6.73	1.22	7.94	0.005
$V-I$	1.02	8	7.74	0.49	9	6.54	1.14	5.32	0.040
$V-J$	2.43	2	0.00	0.00	2	0.00	0.00	4.46	0.563
$R-I$	0.51	8	7.74	0.49	9	6.54	1.14	5.32	0.040
$I-J$	—	0	0.00	0.00	0	0.00	0.00	—	—
$J-H$	0.40	1	6.71	0.00	1	7.88	0.00	—	—
$H-K$	−0.04	1	6.71	0.00	0	0.00	0.00	—	—
S	19.06	10	7.66	0.43	10	6.73	1.22	7.94	0.005

Cubewanos population only									
Color	Cut	Blue Pop.			Red Pop.			Statistics	
		n_1	$\bar{x}$	σ	n_2	$\bar{x}$	σ	f	$prob$
$B-V$	0.93	11	5.83	1.14	12	6.46	0.60	3.63	0.045
$B-R$	1.59	10	5.80	1.11	11	6.55	0.68	2.64	0.146
$B-I$	2.16	9	5.65	1.09	9	6.52	0.71	2.35	0.248
$V-R$	0.63	15	6.04	0.98	15	6.54	0.66	2.23	0.145
$V-I$	1.21	11	5.82	1.07	11	6.46	0.72	2.21	0.227
$V-J$	1.77	2	0.00	0.00	2	0.00	0.00	807.68	0.045
$R-I$	0.61	10	5.66	1.08	11	6.58	0.63	2.93	0.109
$I-J$	—	0	0.00	0.00	0	0.00	0.00	—	—
$J-H$	−0.21	1	4.54	0.00	2	0.00	0.00	—	—
$H-K$	−0.10	1	5.07	0.00	1	4.54	0.00	—	—
S	26.20	12	5.87	1.01	13	6.49	0.70	2.07	0.227
Centaurs and Scattered population only									
Color	Cut	Blue Pop			Red Pop.			Statistics	
		n_1	$\bar{x}$	σ	n_2	$\bar{x}$	σ	f	$prob$
$B-V$	0.91	9	7.73	2.14	10	7.16	2.55	1.42	0.630
$B-R$	1.48	9	7.73	2.14	10	7.16	2.55	1.42	0.630
$B-I$	2.08	8	7.01	2.09	9	7.35	2.63	1.58	0.559
$V-R$	0.57	10	7.72	1.94	10	7.10	2.60	1.81	0.391
$V-I$	1.12	9	7.45	1.83	9	7.08	2.76	2.28	0.266
$V-J$	1.45	2	0.00	0.00	3	7.54	1.28	2.40	0.831
$R-I$	0.55	9	7.65	1.67	10	6.91	2.65	2.52	0.208
$I-J$	0.69	2	0.00	0.00	2	0.00	0.00	14.61	0.326
$J-H$	0.32	2	0.00	0.00	3	6.29	0.98	3.43	0.410
$H-K$	−0.04	2	0.00	0.00	3	7.28	1.46	1.14	0.896
S	20.29	10	7.72	1.94	10	7.10	2.60	1.81	0.391

Table C.3. T-Test (t and $Prob$) for the colors of the various classes: are the mean colors compatible? Note: For each color index, the first line lists the number of objects from both classes considered that are used in the statistics, and the second line gives d and $Prob$. The values of d and $Prob$ that are based on sufficiently large samples to be reliable (i.e. more than 7 objects in each class) are printed in boldface. Only the color indexes for which some computations could be performed are listed.

Color	Pl-QB1	Pl-Cent	Pl-Scat	Pl-Com	QB1-Cent	QB1-Scat	QB1-Com	Cent-Scat	Cent-Com	Scat-Com
$B-V$	20 33	20 15	20 8	20 2	33 15	33 8	33 2	15 8	15 2	8 2
	−1.2 0.238	**−0.6 0.530**	**0.4 0.708**	1.9 0.083	**0.3 0.799**	**1.5 0.151**	3.7 0.009	**0.9 0.367**	2.2 0.049	1.3 0.225
$B-R$	20 30	20 15	20 8	20 2	30 15	30 8	30 2	15 8	15 2	8 2
	−1.3 0.196	**−0.5 0.652**	**0.8 0.435**	1.5 0.188	**0.5 0.638**	**1.8 0.101**	3.2 0.033	**1.1 0.302**	1.6 0.143	0.2 0.844
$B-I$	17 25	17 14	17 7	17 2	25 14	25 7	25 2	14 7	14 2	7 2
	−1.3 0.209	**−0.9 0.397**	**0.3 0.738**	0.8 0.456	**0.1 0.934**	**1.3 0.233**	2.3 0.149	**1.0 0.330**	1.6 0.167	0.3 0.781
$V-R$	20 40	20 15	20 9	20 13	40 15	40 9	40 13	15 9	15 13	9 13
	−1.7 0.097	**−0.2 0.809**	**1.2 0.251**	**3.4 0.003**	**1.0 0.348**	**2.3 0.037**	**4.5 0.000**	**1.2 0.246**	**3.1 0.005**	**1.8 0.091**
$V-I$	17 30	17 13	17 9	17 4	30 13	30 9	30 4	13 9	13 4	9 4
	−1.2 0.225	**−0.5 0.598**	**0.9 0.391**	1.7 0.123	**0.4 0.668**	**1.9 0.076**	3.0 0.026	**1.3 0.225**	2.0 0.069	0.6 0.543
$V-J$	4 5	4 6	4 1	4 0	5 6	5 1	5 0	6 1	6 0	1 0
	2.2 0.069	2.2 0.066	— —	— —	0.0 0.984	— —	— —	— —	— —	— —
$R-I$	17 30	17 14	17 9	17 4	30 14	30 9	30 4	14 9	14 4	9 4
	−1.5 0.138	**−0.8 0.451**	**0.5 0.593**	1.5 0.154	**0.7 0.494**	**2.0 0.070**	3.6 0.009	**1.3 0.226**	2.4 0.034	0.8 0.447
$J-H$	2 4	2 5	2 1	2 0	4 5	4 1	4 0	5 1	5 0	1 0
	1.3 0.364	1.1 0.455	— —	— —	−0.6 0.573	— —	— —	— —	— —	— —
$J-K$	1 3	1 5	1 1	1 0	3 5	3 1	3 0	5 1	5 0	1 0
	— —	— —	— —	— —	−0.4 0.738	— —	— —	— —	— —	— —
$H-K$	1 3	1 5	1 1	1 0	3 5	3 1	3 0	5 1	5 0	1 0
	— —	— —	— —	— —	0.8 0.526	— —	— —	— —	— —	— —
Grt	20 35	20 15	20 9	20 4	35 15	35 9	35 4	15 9	15 4	9 4
	−1.3 0.196	**−0.5 0.596**	**1.0 0.334**	2.0 0.090	**0.5 0.631**	**2.1 0.057**	3.2 0.019	**1.3 0.200**	2.2 0.054	0.8 0.468

Table C.4. t-test applied to the non-physical test classes. Similar tables were obtained for the f and KS tests.

Color	Odd-Even		99-non99	
	Nr per sample	t $Prob$	Nr per sample	t $Prob$
$B-V$	27/26	**0.1 0.948**	9/44	**−0.1 0.894**
$B-R$	25/25	**−0.3 0.758**	7/43	**0.3 0.749**
$B-I$	21/21	**1.0 0.343**	5/37	1.8 0.123
$V-R$	30/30	**−0.5 0.605**	8/52	**−0.1 0.948**
$V-I$	24/23	**−0.3 0.750**	6/41	**1.8 0.108**
$V-J$	5/4	0.2 0.848	0/9	— —
$R-I$	24/23	**−0.1 0.960**	7/40	**2.4 0.033**
$J-H$	3/3	−0.7 0.541	0/6	— —
$J-K$	2/2	−0.6 0.646	0/4	— —
$H-K$	2/2	−0.8 0.569	0/4	— —
Grt	28/27	**0.5 0.636**	8/47	**0.7 0.499**

Table C.5. F-Test for the colors of the various classes: are the color variances compatible?

Color	Pl-QB1	Pl-Cent	Pl-Scat	Pl-Com	QB1-Cent	QB1-Scat	QB1-Com	Cent-Scat	Cent-Com	Scat-Com
$B-V$	20 33	20 15	20 8	20 2	33 15	33 8	33 2	15 8	15 2	8 2
	1.1 0.836	**1.6 0.360**	**1.9 0.381**	24.6 0.315	**1.4 0.406**	**2.1 0.301**	27.2 0.301	**3.0 0.147**	38.5 0.251	12.8 0.424
$B-R$	20 30	20 15	20 8	20 2	30 15	30 8	30 2	15 8	15 2	8 2
	1.1 0.792	**1.8 0.237**	**1.0 0.916**	16.8 0.380	**2.0 0.120**	**1.1 0.768**	15.3 0.401	**1.8 0.452**	30.1 0.284	16.9 0.370
$B-I$	17 25	17 14	17 7	17 2	25 14	25 7	25 2	14 7	14 2	7 2
	1.6 0.305	**1.4 0.515**	**1.0 0.920**	8.5 0.528	**2.2 0.089**	**1.6 0.397**	5.4 0.659	**1.4 0.706**	11.9 0.446	8.5 0.514
$V-R$	20 40	20 15	20 9	20 13	40 15	40 9	40 13	15 9	15 13	9 13
	2.1 0.083	**2.3 0.098**	**1.6 0.361**	**2.4 0.088**	**1.1 0.822**	**1.3 0.743**	**1.1 0.736**	**1.4 0.658**	**1.1 0.919**	**1.5 0.606**
$V-I$	17 30	17 13	17 9	17 4	30 13	30 9	30 4	13 9	13 4	9 4
	1.1 0.756	**1.3 0.634**	**1.0 0.913**	3.1 0.387	**1.4 0.407**	**1.2 0.717**	2.7 0.446	**1.2 0.774**	3.9 0.287	3.1 0.375
$V-J$	4 5	4 6	4 1	4 0	5 6	5 1	5 0	6 1	6 0	1 0
	5.4 0.198	6.7 0.148	— —	— —	1.2 0.856	— —	— —	— —	— —	— —
$R-I$	17 30	17 14	17 9	17 4	30 14	30 9	30 4	14 9	14 4	9 4
	1.4 0.451	**1.4 0.508**	**1.4 0.681**	5.9 0.169	**1.1 0.954**	**1.0 0.906**	4.3 0.252	**1.1 0.883**	4.1 0.273	4.4 0.254
$J-H$	2 4	2 5	2 1	2 0	4 5	4 1	4 0	5 1	5 0	1 0
	2.5 0.419	**** 0.001	— —	— —	48.6 0.003	— —	— —	— —	— —	— —
$J-K$	1 3	1 5	1 1	1 0	3 5	3 1	3 0	5 1	5 0	1 0
	— —	— —	— —	— —	9.5 0.060	— —	— —	— —	— —	— —
$H-K$	1 3	1 5	1 1	1 0	3 5	3 1	3 0	5 1	5 0	1 0
	— —	— —	— —	— —	35.1 0.006	— —	— —	— —	— —	— —
Grt	20 35	20 15	20 9	20 4	35 15	35 9	35 4	15 9	15 4	9 4
	1.3 0.537	**1.5 0.403**	**1.1 0.979**	2.9 0.409	**1.1 0.716**	**1.4 0.643**	3.8 0.293	**1.6 0.508**	4.4 0.248	2.7 0.439

Table C.6. KS Test for the colors of the various classes: are the distribution compatible?

Color	Pl-QB1	Pl-Cent	Pl-Scat	Pl-Com	QB1-Cent	QB1-Scat	QB1-Com	Cent-Scat	Cent-Com	Scat-Com
$U-B$	0 1	0 0	0 1	0 0	1 0	1 1	1 0	0 1	0 0	1 0
	— —	— —	— —	— —	— —	1.0 0.289	— —	— —	— —	— —
$U-V$	0 1	0 0	0 1	0 0	1 0	1 1	1 0	0 1	0 0	1 0
	— —	— —	— —	— —	— —	1.0 0.289	— —	— —	— —	— —
$U-R$	0 1	0 0	0 1	0 0	1 0	1 1	1 0	0 1	0 0	1 0
	— —	— —	— —	— —	— —	1.0 0.289	— —	— —	— —	— —
$U-I$	0 1	0 0	0 1	0 0	1 0	1 1	1 0	0 1	0 0	1 0
	— —	— —	— —	— —	— —	1.0 0.289	— —	— —	— —	— —
$B-V$	20 33	20 15	20 8	20 2	33 15	33 8	33 2	15 8	15 2	8 2
	0.2 0.788	**0.3 0.508**	**0.2 0.895**	0.6 0.353	**0.2 0.619**	**0.4 0.217**	0.7 0.146	**0.4 0.269**	0.5 0.517	0.6 0.366
$B-R$	20 30	20 15	20 8	20 2	30 15	30 8	30 2	15 8	15 2	8 2
	0.4 0.081	**0.3 0.508**	**0.2 0.895**	0.5 0.585	**0.3 0.173**	**0.5 0.079**	0.8 0.085	**0.4 0.291**	0.5 0.517	0.5 0.651
$B-I$	17 25	17 14	17 7	17 2	25 14	25 7	25 2	14 7	14 2	7 2
	0.4 0.048	**0.3 0.584**	**0.2 0.989**	0.5 0.670	**0.3 0.300**	**0.4 0.283**	0.8 0.120	**0.4 0.271**	0.6 0.433	0.6 0.494
$V-R$	20 40	20 15	20 9	20 13	40 15	40 9	40 13	15 9	15 13	9 13
	0.3 0.148	**0.2 0.763**	**0.2 0.793**	**0.5 0.012**	**0.3 0.327**	**0.4 0.098**	**0.6 0.000**	**0.4 0.389**	**0.5 0.023**	**0.3 0.539**
$V-I$	17 30	17 13	17 9	17 4	30 13	30 9	30 4	13 9	13 4	9 4
	0.3 0.222	**0.2 0.975**	**0.3 0.692**	0.5 0.350	**0.3 0.230**	**0.5 0.034**	0.7 0.021	**0.3 0.539**	0.5 0.229	0.2 0.996
$V-J$	4 5	4 6	4 1	4 0	5 6	5 1	5 0	6 1	6 0	1 0
	0.8 0.082	0.7 0.135	1.0 0.150	— —	0.5 0.454	0.8 0.362	— —	0.7 0.583	— —	— —
$R-I$	17 30	17 14	17 9	17 4	30 14	30 9	30 4	14 9	14 4	9 4
	0.3 0.152	**0.2 0.688**	**0.2 0.802**	0.5 0.350	**0.3 0.420**	**0.5 0.034**	0.7 0.021	**0.4 0.234**	0.6 0.123	0.3 0.907
$J-H$	2 4	2 5	2 1	2 0	4 5	4 1	4 0	5 1	5 0	1 0
	0.8 0.242	0.8 0.158	1.0 0.201	— —	0.6 0.357	0.8 0.461	— —	0.6 0.724	— —	— —
$J-K$	1 3	1 5	1 1	1 0	3 5	3 1	3 0	5 1	5 0	1 0
	0.7 0.641	0.6 0.724	1.0 0.289	— —	0.7 0.224	0.7 0.641	— —	0.8 0.362	— —	— —
$H-K$	1 3	1 5	1 1	1 0	3 5	3 1	3 0	5 1	5 0	1 0
	0.7 0.641	0.8 0.362	0.1 1.000	— —	0.3 0.947	0.7 0.641	— —	0.8 0.362	— —	— —
Grt	20 35	20 15	20 9	20 4	35 15	35 9	35 4	15 9	15 4	9 4
	0.3 0.115	**0.2 0.678**	**0.2 0.837**	0.4 0.389	**0.3 0.386**	**0.5 0.016**	0.7 0.025	**0.3 0.561**	0.5 0.225	0.2 0.996

References

Asher, D. J., & Steel, D. I. 1999, MNRAS, 263, 179

Barucci, M. A., Doressoundiram, A., Tholen, D., Fulchignoni, M., & Lazzarin, M. 1999, Icarus, 142, 476

Barucci, M. A., Fulchignoni, M., Birlan, M., et al. 2001, A&A, 371, 1150

Barucci, M. A., Romon, J., Doressoundiram, A., & Tholen, D. J. 2000, AJ, 120, 496

Binzel, R. P. 1992, Icarus, 99, 238

Boehnhardt, H., Tozzi, G. P., Birkle, K., et al. 2001, A&A, 378, 653

Brown, R. H., Cruikshank, D. P., & Pendleton, Y. 1999, AJ, 519, L101

Brown, R. H., Cruikshank, D. P., Pendleton, Y., & Veeder, G. J. 1998, Science, 280, 1430

Brown, W. R., & Luu, J. X. 1997, Icarus, 126, 218

Buie, M. W., & Bus, S. J. 1992, Icarus, 100, 288

Campins, H., Rieke, G. H., & Lebofsky, M. J. 1985, AJ, 90, 896

Consolmagno, G. J., Tegler, S. C., Rettig, T., & Romanishin, W. 2000, Bull. Am. Astron. Soc., 32

Cox, A. N. 2000, Allen's Astrophysical Quantities (New York: Springer)

Davies, J. 2001, Beyond Pluto (Cambridge: Cambridge University Press)

Davies, J. K. 2000, in Minor Bodies in the Outer Solar System, ed. A. Fitzsimmons, D. Jewitt, & R. M. West (Springer), 9

Davies, J. K., Green, S., McBride, N., et al. 2000, Icarus, 146, 253

Davies, J. K., McBride, N., Ellison, S. L., Green, S. F., & Ballantyne, D. R. 1998, Icarus, 134, 213

Davis, D. R., & Farinella, P. 1997, Icarus, 125, 50

Delahodde, C. E., Meech, K. J., Hainaut, O. R., & Dotto, E. 2001, A&A, 376, 672

Delsanti, A. C., Boehnhardt, H., Barrera, L., et al. 2001, A&A, 380, 347
Doressoundiram, A., Barucci, M. A., Romon, J., & Veillet, C. 2001, Icarus, 154, 277
Farinella, P., & Davis, D. R. 1996, Science, 273, 938
Ferrin, I., Rabinowitz, D., Schaefer, B., et al. 2001, AJ, 548, L243
Fink, U., Hoffmann, M., Grundy, W., Hicks, M., & Sears, W. 1992, Icarus, 97, 145
Gil-Hutton, R., & Licandro, J. 2001, Icarus, 152, 246
Gladman, B., Kavelaars, J. J., Nicholson, P. D., Loredo, T. J., & Burns, J. A. 1998, AJ, 116, 2042
Green, S. F., McBride, N., O Ceallaigh, D. P., et al. 1997, MNRAS, 290, 186
Gutiérrez, P. J., Ortiz, J. L., Alexandrino, E., Roos-Serote, M., & Doressoundiram, A. 2001, A&A, 371, L1
Hahn, J. 2000, Lunar & Planetary Sci. Conf. 31, 1797
Hahn, J., & Malhotra, R. 1999, AJ, 117, 3041
Hainaut, O. R. 2001, Priv. Comm.
Hainaut, O. R., Delahodde, C. E., Böhnhardt, H., et al. 2000, A&A, 356, 1076
Hardorp, J. 1980, A&A, 88, 334
Jewitt, D. 2002, AJ, in press
Jewitt, D., & Kalas, P. 1998, AJ, 499, L103
Jewitt, D., & Luu, J. 1998, AJ, 115, 1667
Jewitt, D. C. 1992, Special session at D.P.S., Munich
Jewitt, D. C., & Luu, J. X. 1992, IAU Circ., 5611
Jewitt, D. C., & Luu, J. X. 1998, AJ, 115, 1667
Jewitt, D. C., & Luu, J. X. 2001, AJ, 122, 2099
Jewitt, D. C., & Meech, K. J. 1986, AJ, 310, 937
Kowal, C. 1977, IAU Circ., 3129
Kowal, C., Liller, W., & Marsden, B. 1979, IAU Symp., 81, 245
Landolt, A. 1992, AJ, 104, 340
Luu, J., & Jewitt, D. 1996a, AJ, 112, 2310
Luu, J., & Jewitt, D. C. 1996b, AJ, 111, 499
Malhotra, R. 1995, AJ, 110, 420
Malhotra, R. 1996, AJ, 111, 504
McBride, N., Davies, J. K., Green, S. F., & Foster, M. J. 1999, MNRAS, 306, 799
Meech, K. J., & Belton, M. J. S. 1989, IAU Circ., 4770
Meech, K. J., Hainaut, O. R., & Marsden, B. G. 2002, Icarus, submitted
Morbidelli, A. 2001, in TNO International Meeting, Meudon, June 2001
Mueller, B. E. A., Tholen, D. J., Hartmann, W. K., & Cruikshank, D. P. 1992, Icarus, 97, 150
N., McBride, J. K., Davies, S. F. G., & Foster, M. J. 1999, MNRAS, 306, 799
Parker, J. 2001, Distant EKO, URL `http://www.boulder.swri.edu/ekonews/`
Parker, J. W., Stern, S. A., Festou, M. C., A'Hearn, M. F., & Weintraub, D. 1997, AJ, 113, 1899
Peixinho, N., Lacerda, P., Ortiz, J. L., et al. 2001, A&A, 371, 753
Press, W., Teukolsky, S., Vetterling, W., & Flannery, B. 1992, Numerical Recipes in FORTRAN (UK: Cambridge University Press)
Romanishin, W., & Tegler, S. C. 1999, Nature, 398, 129
Romanishin, W., Tegler, S. C., Levine, J., & Butler, N. 1997, AJ, 113, 1893
Russell, H. N. 1916, AJ, 43, 173
Sekiguchi, T., Böhnhardt, H., Hainaut, O. R., & Delahodde, C. E. 2002, A&A, 385, 281
Stern, S. A. 1996, AJ, 112, 1203
Strazzula, G. 1998, Solar System Ices, ed. B. Schmitt, C. de Bergh, & M. Festou (Netherlands: Kluwer), 281
Strazzula, G., & Johnhson, R. 1991, Comets in the Post-Halley Era, ed. R. L. Newburn, M. Neugebauer, & J. Rahe (Dordrecht: Kluwer), 243
Tegler, S. C., & Romanishin, W. 1998, Nature, 392, 49
Tegler, S. C., & Romanishin, W. 2000, Nature, 407, 979
Tholen, D. J., Hartmann, W. K., & Cruikshank, D. P. 1988, IAU Circ., 4554
Thompson, W. R., Murray, B. G. J. P. T., Khare, B. N., & Sagan, C. 1987, J. Geophys. Res., 92, 14933
Trujillo, C., Bouchez, A., & Brown, M. 2001, in TNO International Meeting, Meudon, June 2001
Weintraub, D. A., Tegler, S. C., & Romanishin, W. 1997, Icarus, 128, 456